AN AUTOMATED DOSIMETRY SYSTEM
FOR COMPUTED TOMOGRAPHY X-RAY SCANNERS
USING SILICON P-I-N DIODES

BY

JOHN JOSEPH LANZA

A DISSERTATION PRESENTED TO THE GRADUATE COUNCIL OF THE
UNIVERSITY OF FLORIDA
IN PARTIAL FULFILLMENT OF THE REQUIREMENTS FOR THE DEGREE OF
DOCTOR OF PHILOSOPHY

UNIVERSITY OF FLORIDA

1979

ACKNOWLEDGMENTS

I would like to thank the members of my supervisory committee for their invaluable assistance in completing my degree requirements. Dr. Walter Mauderli, my chairman, has successfully guided me through many trying times while working on the project. Dr. Genevieve Roessler, my co-chairman, deserves special recognition because she was responsible for my entering the field of radiation physics and for sponsoring a research assistantship during the first three years of my graduate work. Dr. Lawrence Fitzgerald was always willing to answer my questions any time. Dr. Frank Agee allowed me to work with the CT scanner in Neuro-radiology. Dr. Eugene Chenette was my first contact at the University six years ago and quickly agreed to substitute for another member of the original committee.

Special thanks go to Howard Brown, Ken Fawcett, Joe Mueller, and Charles Rabbit for providing technical assistance during the course of the project.

The Bureau of Radiological Health was responsible for the funding that allowed me to complete these studies. I appreciate the guidance of Bill Properzio, Tommy Morgan, and Tom Lee at the Bureau.

I would like to thank my friend, Dr. John Stampelos, for special understanding during this work.

Finally, I would like to thank my typist for the patience she has shown me in previous papers.

TABLE OF CONTENTS

LIST OF TABLES

LIST OF FIGURES

Abstract of Dissertation Presented to the Graduate Council
of the University of Florida in Partial Fulfillment of the Requirements
for the Degree of Doctor of Philosophy

AN AUTOMATED DOSIMETRY SYSTEM
FOR COMPUTED TOMOGRAPHY X-RAY SCANNERS
USING SILICON P-I-N DIODES

By

John Joseph Lanza

March, 1979

Chairman: Walter Mauderli, D. Sc.
Co-Chairman: Genevieve S. Roessler, Ph.D
Major Department: Nuclear Engineering Sciences

A dosimetry system for computed tomography (CT) x-ray scanners has

been developed featuring X-Y as well as Z-axis directional exposure

measurement capabilities. The device is unique because it uses an ar-

ray of closely spaced silicon p-i-n diodes as radiation detectors. This

arrangement allows detailed mapping of dose levels along the length of

the detector module.

Computed tomography scanners are a new generation of diagnostic

radiology devices using highly collimated x-ray beams that pass through

a body section axially. The photons not absorbed are detected (depend-

ing on the manufacturer's model) by scintillating crystals, ionization

chambers, or semiconductor materials, and their number is a function of

the density of the material they must traverse. The x-ray tube and

detectors generally rotate in unison at opposite sides around the

patient while collecting absorption data for later reconstruction by

computer and display.

Prior to the development of this dosimeter, no simple and convenient method was available for performing exposure distribution measurements on CT scanners. Previous measurement methods have included the use of photographic film, pencil-type ionization chambers, or an array of as many as 300 to 500 thermoluminescent dosimeter chips. Silicon diodes are superior to these methods because of their small size, higher photon stopping power, linear energy response, and minimal x-ray beam directional dependence.

The system described features 25 evenly spaced silicon diode detectors each with its own current-to-voltage converter. The amplified output from each diode is transferred to the data handling module that integrates the signal and provides permanent storage via a thermal printer. Calibration factors can be applied allowing the readout to correspond to the radiation exposure in Roentgens received by the diodes during the course of a CT scan. The dynamic range of the instrument enables it to measure exposures in fields as high as 100 R/sec and to present the integrated exposure information in three ranges of 0-1, 10, and 100 R.

CHAPTER I
INTRODUCTION

The field of diagnostic radiology began in 1895 shortly after the discovery of x-rays by Roentgen (Jo74). During the past three quarters of a century improvements have been made in both techniques and equipment but, until a few years ago, there were really no major advances in diagnostic x-ray procedures.

A revolution was started in 1967 when Hounsfield of EMI Limited developed a new x-ray transmission system--the computed axial tomography scanner or CT scanner (Ho73). The CT system possessed features novel to radiology, including:

1. X-ray beams that are highly collimated to reduce scatter contributions;

2. The use of solid-state scintillation detectors possessing high signal-to-noise ratios;

3. The use of mathematical reconstruction techniques to solve for the attenuation coefficients of the tissues of interest, thereby revealing adjacent areas of slightly varying density; and

4. The presentation of the radiologic image as an axial slice, thus, eliminating the obscuration of detail due to overlapping tissues as is currently found in conventional radiography.

The introduction of the CT scanner has greatly affected health care delivery because of these unique characteristics. In many clinical situations, because of its ease of use, non-invasive technique, and lack of need for inpatient care, the CT scan has replaced many common radiological procedures such as arteriograms, pneumoencephalograms, and some nuclear medicine examinations (Tu77;Ba76;Ev78;Li75;Fi77).

1

The basic technique of CT calls for a highly collimated x-ray beam to pass through a body section axially. The first units could scan only the head but now scanners are available that can view all areas of the body. The photons not absorbed in body tissues are detected, depending on the model, by scintillating crystals, ionization chambers, or by semiconductor materials and their number is a function of the density of the material they must traverse (CT77;Va77;Se76;As76). In most current units, the x-ray tube and the detectors rotate in unison at opposite sides around the patient while collecting absorption data for later reconstruction and display. The earliest CT system took as long as five minutes to complete one scan. Now, however, units are being produced with scan times as low as one or two seconds (Le76;Pi78). Sub-second scanners are presently on the drawing boards.

In 1973, the first EMI head units were installed in hospitals in the United States (Co76). Since then, over 760 units of both types have been sold in this country (Com77). Presently, more than ten companies are either manufacturing or designing CT scanning systems.

Extensive research has been undertaken in hopes of improving resolution, scan speed, and data handling in CT systems (Go77a). Patient radiation dosimetry is one area, however, that has not, as yet, been definitively studied (Co76;Cl76;Ta77;Bur77;Co77). In the past history of diagnostic radiology, misapplication of x-rays often resulted in dramatic biological effects including leukemia and various neoplasms. The full impact of the deleterious effects of the radiation exposure, in many cases, was not realized until years later. Preliminary studies on CT scanners indicate patient dosage varies as to (Ba76;Mc75;Ba77;Mc74;Ph75a; Ph75b;We77;Mc76;Pe73):

1. Scan time;

2. Number of slices taken;

3. Picture element size in the reconstructed matrix;

4. Slice thickness; and

5. The voltage and current settings of the x-ray tube on a particular unit.

A normal CT procedure usually consists of between five and ten contiguous scans of a particular region of the body. Most units have the feature of viewing two slightly overlapping sections or slices per scan (Le74;Oh76a;CT76). Scan widths in many units can be varied between 3mm and 15mm per slice (Va76;Se76). Skin doses in excess of five rads per scan have been measured from some CT models (Oh76b;Mc76;Sho78). It must be pointed out, however, that the exposure per scan is to a small area of the body. This is in contrast to conventional radiological studies where the dose is larger due to a higher scatter component. From these considerations, integrated doses over the entire area of the scan may add up to skin doses as high as 25 rads or more (We77). Internal doses are smaller but still appreciable (Mc76).

The "Radiation Control for Health and Safety Act" (PL 90-602) was issued to set standards that would act to reduce human exposure from x-ray equipment (including CT scanners) (Re76). Numerous states have established boards to determine standards and criteria for CT scanner acquisition which includes the requirement that patient radiation exposures be minimized while realizing the risk-benefit considerations of diagnostic radiology (Cl76;St77). Adequate health care planning and delivery must include a quantitative assessment of radiation exposure patients can be expected to receive during normal x-ray procedures. If adequate dosimetric studies can be performed during the infancy of CT

scanning, questions and criticisms as to the usefulness of this type of procedure can be accurately evaluated.

Presently the Bureau of Radiological Health (BRH) is developing regulations to modify or replace the performance standard for "Diagnostic X-ray Systems and Their Major Components" (21CFR1020.30). At the moment, CT scanners must uphold the minimum design and operational requirements set for conventional diagnostic x-ray machines. Because of the unique technology presented by the CT device, standards must be designed to permit maximum patient medical benefit with a minimum obligatory radiation exposure risk (Sc78;Co78;Pr78).

Dosimetric studies performed on CT scanners up to this time have used photographic film, thermoluminescent dosimeters(TLD), or ion chambers as the radiation detectors (Ca77;Mo77;De78). In a continuing study, the BRH is conducting in-depth dosimetric research using as many as 500 TLD dosimeters placed inside a Plexiglas phantom. This technique proves to be both tedious and expensive. At the moment, however, it is the most expeditious means of obtaining dose profile information.

The project described involved the design and construction of a portable radiation dosimetry system for CT scanner operations. Present phantoms for CT systems were intended mainly to measure only the image quality of the various units available (Go77a;Al77;HT76). The device constructed consists of a Plexiglas module containing 25 serially spaced silicon diodes that are used as the radiation detectors (Figure 1). This arrangement allows for the measurement of exposures at selected points along the length of the diode module. The output of each diode detector feeds into an amplifier that converts the photocurrent into a voltage. This voltage signal is then sent to the control/readout module that contains the circuits necessary for data integration and display. The final
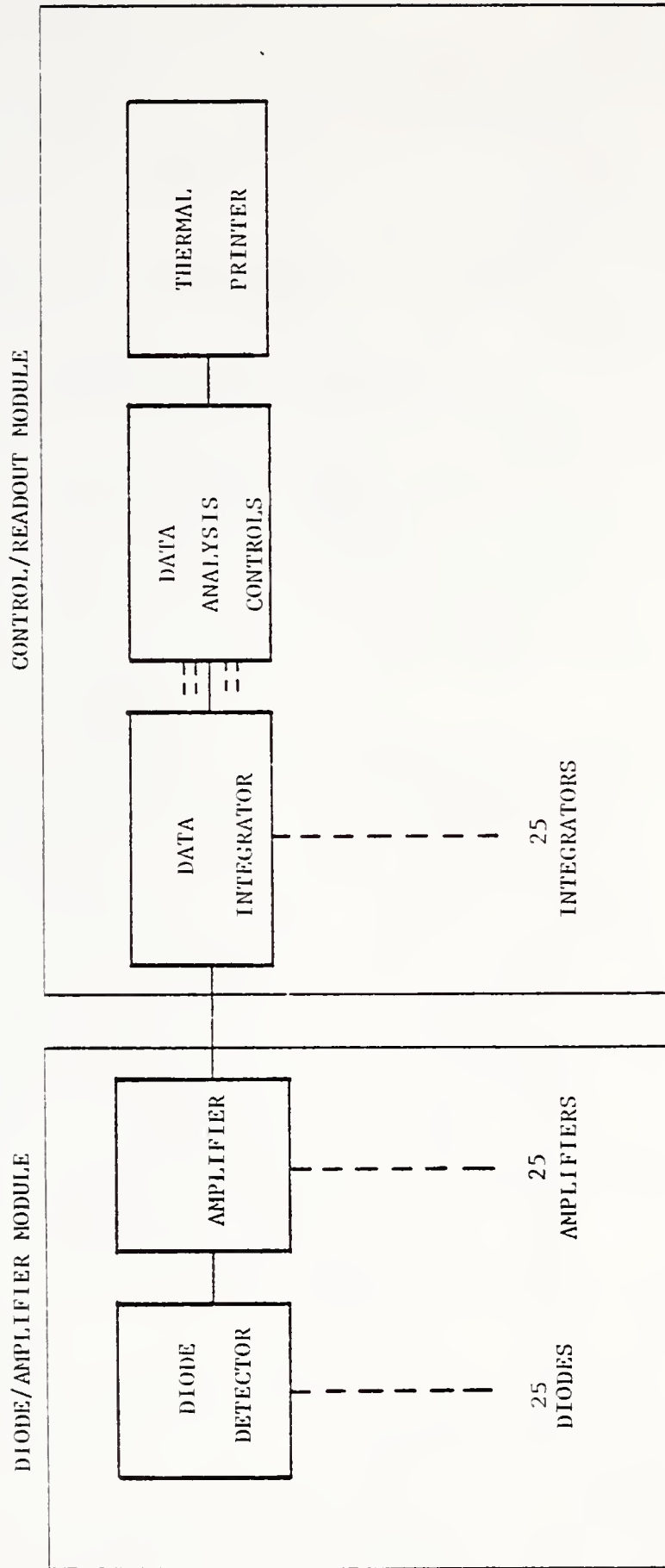
FIGURE 1. BLOCK DIAGRAM OF DOSIMETRY SYSTEM

readout is in a form that, after applying appropriate calibration factors, indicates the radiation exposure received by the detectors during the CT scan. The dynamic range of the instrument enables it to measure exposures in x-ray fields as intense as 100 R/sec and to present the integrated exposure information in three ranges, namely, 0-1, 10, and 100 R.

The term "exposure" rather than dose will be used in describing the actual experimental results obtained from the dosimeter because the device is calibrated so that the output of any detector is proportional to the ionization in air for photons in the energy range produced by CT scanners.

CHAPTER II
BACKGROUND AND RELATED RESEARCH

Developmental Review

Before a discussion of CT dosimetry can be undertaken, a brief re-
view of the principles behind the development of computerized tomography
should be presented. The major difference between computed tomography
and conventional diagnostic radiological techniques is that CT uses
mathematical recombination methods to produce the desired radiological
image. The mathematical basis for these techniques was essentially
developed by Radon in 1917 (Ka77). Bracewell, in 1956, improved these
ideas and applied them to solar radioastronomy (Br76). The first medical
application of image reconstruction was done by Oldendorf in 1961 and by
Kuhl and Edwards in 1963 (In76). It was not until 1967, however, that
the first clinically useful instrument was produced by Hounsfield of
EMI Limited in England (Ho73).

Although a number of variations have been developed, there are really
only three basic types or generations of CT scanners. The first genera-
tion, of course, is exemplified by the original EMI head scanner. It
consisted of an x-ray source and a pair of sodium iodide detectors (Ho73).
The x-ray source emitted a pencil beam of radiation that passed through the
patient as the source translated laterally (Figure 2). The detectors
moved in synchrony with the source on the opposite side of the patient.
At the end of the lateral pass, the whole assembly rotated one degree.
This rotation and lateral translation process repeated until a 180° arc
had been completed. Nominally, one scan took about five minutes to
complete.

7
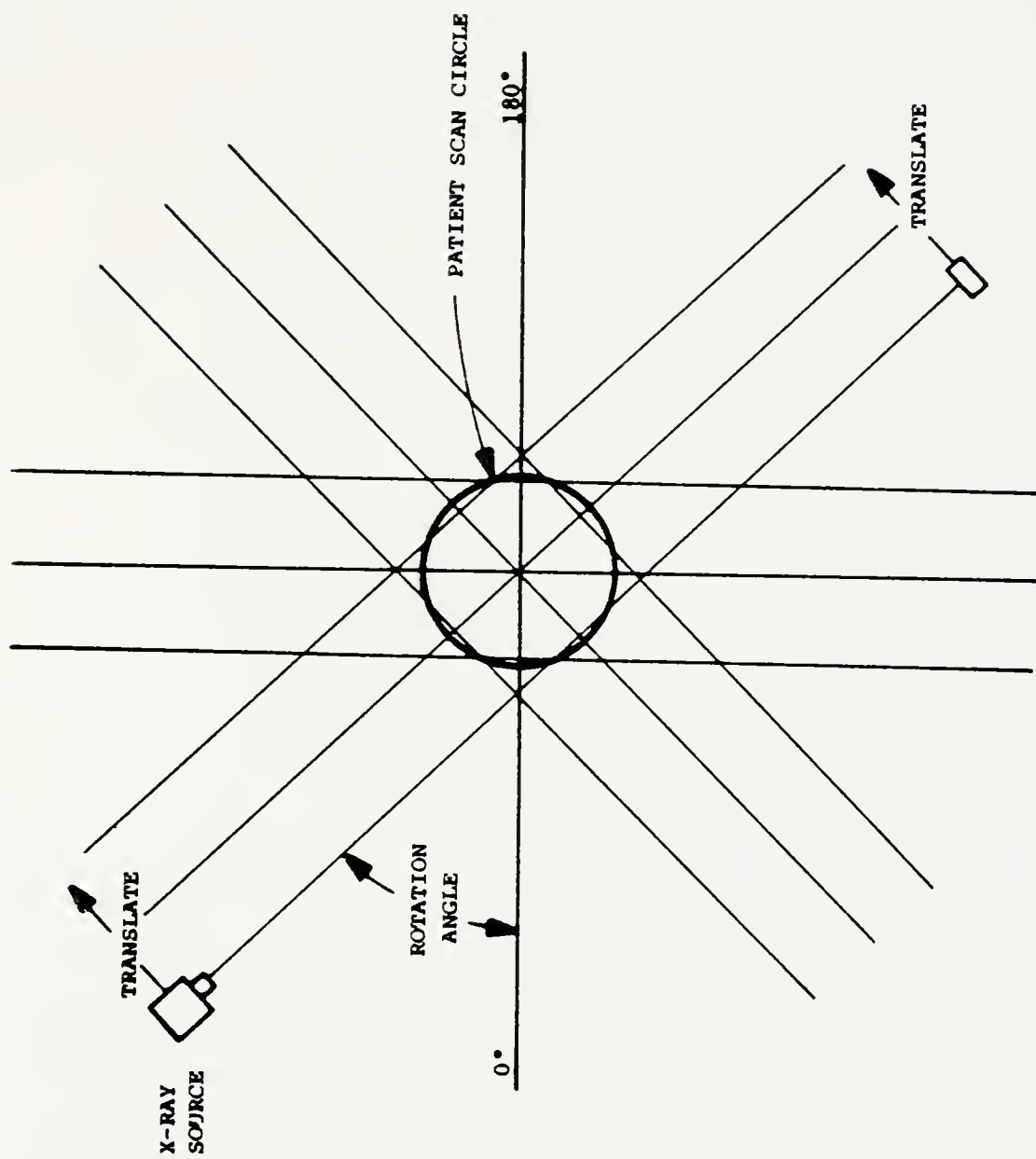
FIGURE 2. FIRST GENERATION CT SCANNER

The second generation scanner featured one or more sources with multiple detectors (Figure 3). The lateral translation and rotation (180°) were still present except that the angular motion was larger. This improvement brought scan times down to about one minute.

Computed tomography's third generation of machines consisted of a continuously rotating (360°), pulsed, fan beam source with an array of detectors on the far side of the patient (Figure 4) (Ge77;CT78). Manufacturers have used xenon-filled ionization chambers as well as silicon diodes as the detectors in these devices. A variation on this method involves placing stationary detectors on the full 360° scan circumference. Scan times have been reduced to as low as one or two seconds by some manufacturers (Pi78;Oh76c).

As the x-ray beam sweeps through body tissue, those photons not absorbed are detected and a record of their magnitude is stored on magnetic discs. Image reconstruction involves the mathematical recombination of all the sweeps from every angle made through the subject. In raw form, a computer prints out numbers (Hounsfield units) that are proportional to the average linear attenuation coefficient for a small volume of tissue relative to water. These numbers are usually converted to a shade of gray and then displayed on a cathode ray tube as a picture element or pixel. The resulting image is an axial view of a body section as if an individual were viewing a cross section of the patient from below. The size of the picture matrix may vary from 80 x 80 to 512 x 512 pixels depending on predetermined objectives and the type of machine used.

It should be emphasized that the pixel is really a three-dimensional concept represented in two-dimensions (X-Y) and its magnitude or shade of gray is obtained from the summation of the relative attenuation
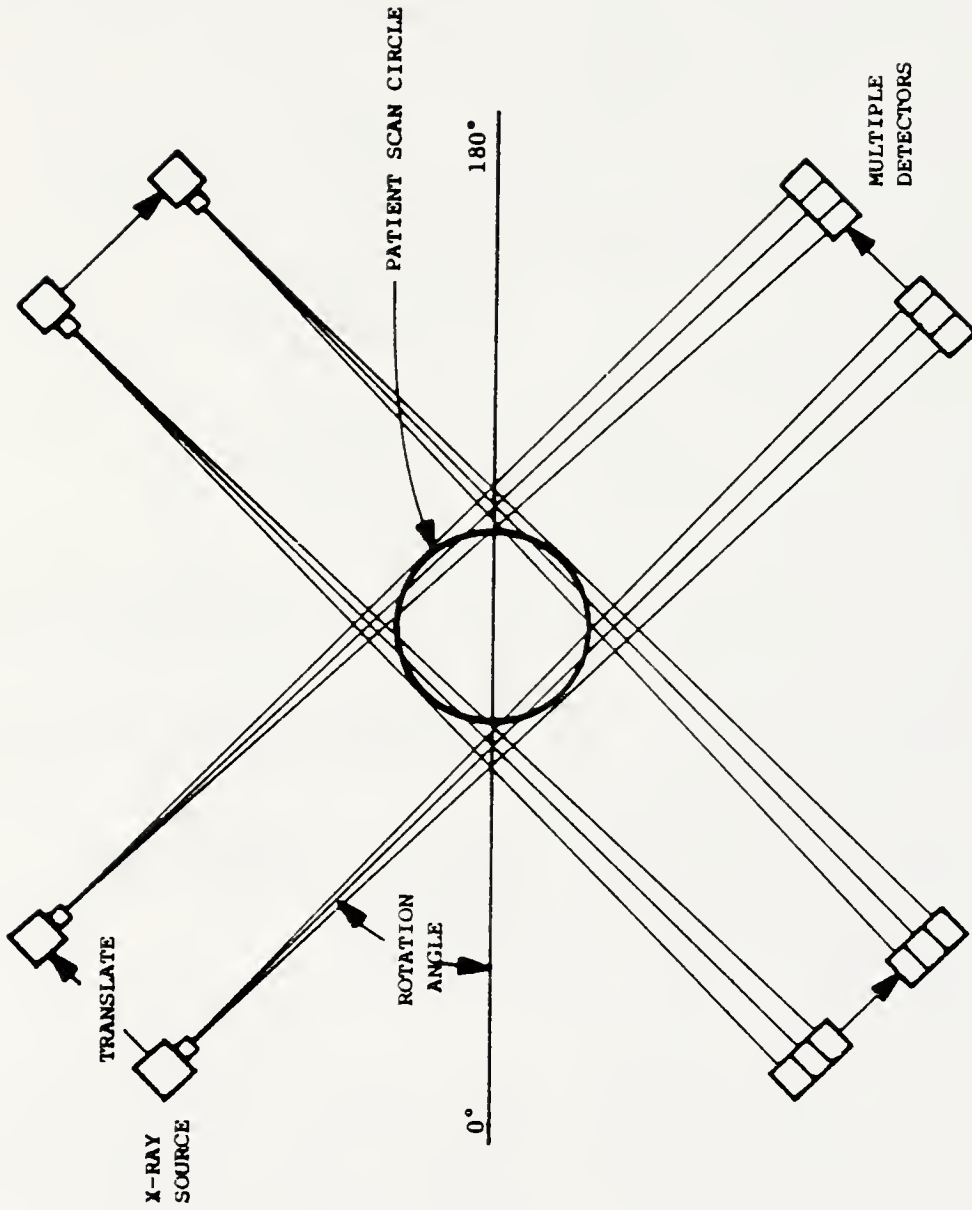
FIGURE 3. SECOND GENERATION CT SCANNER
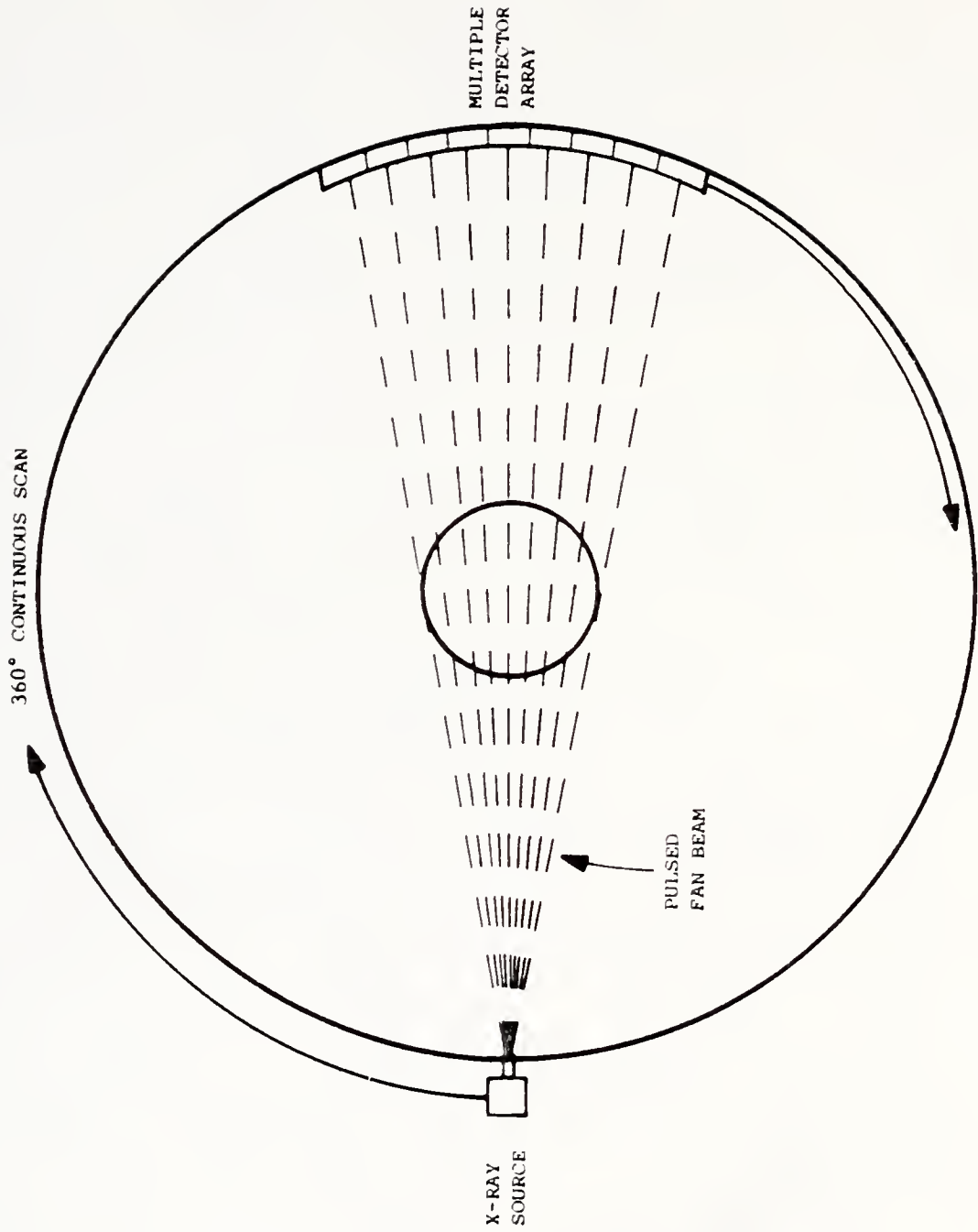
FIGURE 4. THIRD GENERATION CT SCANNER

coefficients for a particular tissue volume (Figure 5). The thickness of the scan (beam width) in the Z-direction is finite and indicates the geometrical width of a single slice at the center of the patient (Th78). In current machines, this dimension per slice can be varied from 3 to about 15 mm by collimation at the source and the detectors. The X and Y-dimensions in the reconstructed image are a function of the matrix size and of the reconstruction (lateral) distance scanned (Pa76).

Dose Considerations

A discussion of dose considerations in CT scanning procedures must review a variety of factors that tend to be variable depending on the manufacturer of the particular CT unit in question and the method of dose measurement. An overview of some of these considerations would include paragraphs on x-ray tube characteristics, signal-to-noise considerations in the detecting systems, and a description of present CT dose measurement techniques.

Radiation Sources

Currently, almost all commercial CT scanners use x-ray tubes as their radiation source since these devices exhibit high contrast/resolution scanning with a minimum of shielding problems (Mc77). Radionuclide scanners are actively being developed (Mo77;De77a;De77b;Ge77;Bu77;Cho77) and at least one manufacturer (Un78) has marketed a workable unit. The two types of tubes that are generally used in present scanners are off-the-shelf varieties with few, special, CT scan-added features.

Tubes that are used in lateral translate-rotation systems are oil-cooled types with a fixed anode and line focus (2 x 16 mm focal spot). They are operated at between 100 and 160 kVp at a tube current so as not to exceed a 4000 kVp·mA heat loading. These tubes are of the three phase
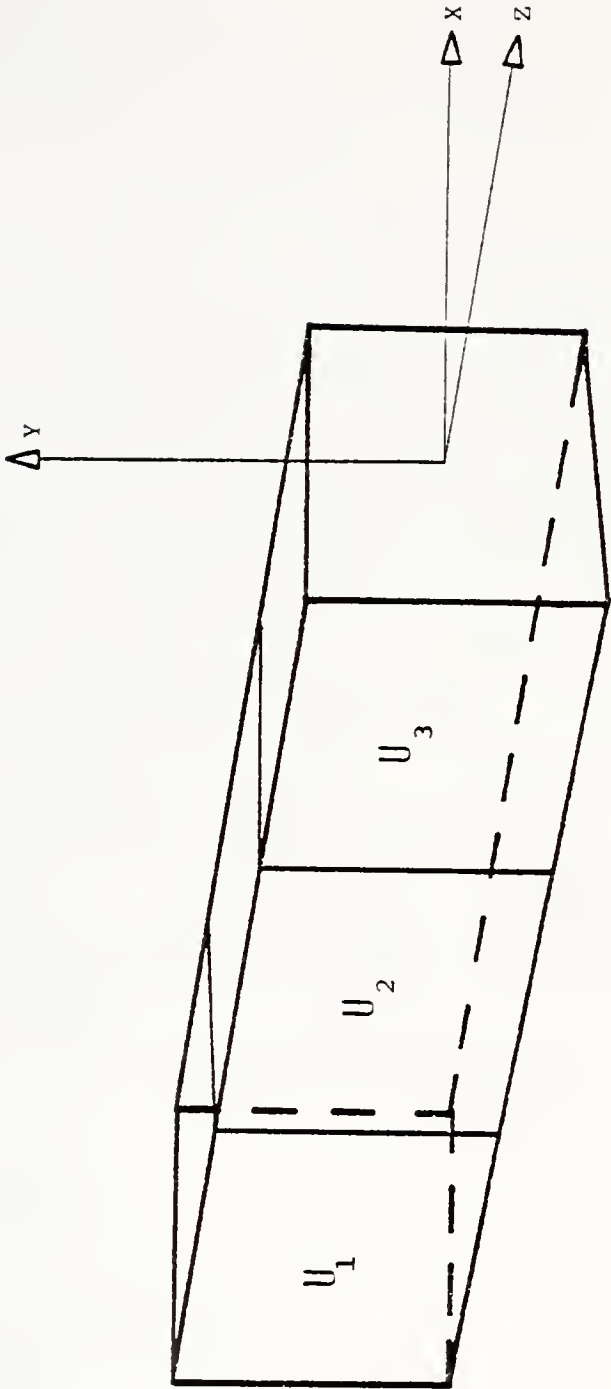
FIGURE 5. PIXEL, GRAY SCALE $\propto U_1 + U_2 + U_3$ REPRESENTED
AS A SINGLE SHADE OF GRAY ON THE IMAGE MONITOR

constant potential-type. The output of these tubes is polychromatic with average energies between 40-50 keV prior to entering the patient. The effective energy of the beam is generally higher than the mean depending on the inherent and added filtration incorporated by each manufacturer. For example, in the EMI head scanner operated at 120 kVp, 32 mA with 4.4 mm Al total filtration, the effective photon energy is 73 keV (Mc77).

Almost all of the manufacturers of sub-ten second rotational scanners (fan beam) use a pulsed, rotating anode x-ray tube (Mc77). These tubes are air-cooled and have a small focal spot of about 0.6 mm. Pulsed tubes are operated at kVp's similar to fixed anode sources but use currents up to 500 mA producing pulses of 2-3 msec in length. Because of their 360° angular motion, fan beam devices produce a more homogeneous dose distribution since every point in the subject is exposed to the primary beam for similar periods of time.

Radiation Energy

A number of factors modify the x-ray beam energies utilized during a CT scan (Pe77;Za77). Higher energy beams, in general, are better transmitted through the subject. Their use leads to better photon statistics and, usually, lower surface dose. However, lower energy radiation has characteristically higher attenuation coefficients and, therefore, slight differences in tissue density can be more readily observed. The polychromaticity of the x-ray source tends to integrate these effects. This range of energies in itself, though, means that due to filtration of the beam by the subject, the x-ray spectrum hardens as the depth of transmission increases.

In general, radiation dose distributions vary considerably depending on subject characteristics such as size, shape and density (Jo74). The clinician would normally scan infants using lower energies such as

100 kVp radiation because of their small cross section (Ag78). This would produce higher skin doses but lower internal dose levels. Large or obese adults would receive radiations of maximum energy usually between 130 and 140 kVp. In this case, the skin dose will be lowered but internal dose values would increase. Scattered radiation also contributes to the total dose. Forward scatter is relatively independent of energy, whereas side scatter is greater for lower energies (Jo74). Thus, even with adequate collimation, the scatter component could contribute a sizeable fraction of the total dose.

It must be emphasized, that the clinician can greatly determine total patient dose not only by limiting the number of scans but also by using the most advantageous energy in a particular situation.

System Noise

The CT image is displayed in different shades of gray on an image monitor or as printed digital data representing the relative attenuation coefficients of the material through which the x-ray beam passed. The image consists of a matrix of pixels corresponding to the density of volume elements of the scanned material. The ability to recognize two closely spaced volume elements of similar density depends on the resolution of the system and on the minimum pixel size. System noise due to statistical fluctuations in the photon flux delineates the lower level of resolution and the upper limits of the matrix size allowable (Ba77; Go77b;Mot78;Ch77;Pa76;Ju77;Ba76).

Generally, to decrease the photon-induced noise significance, the magnitude of the photon flux must be increased. This can be done by operating the x-ray tube at a higher kVp, however, that also increases the internal dose. Brooks and Di Chiro (Br76) have developed an expression describing the relationship between noise, resolution, and patient

dose. The variance, σ^2, of the reconstructed attenuation coefficients due to noise is given by:

$$\sigma^2(\mu) \propto \frac{\gamma\,\beta}{\omega^3 h\, D_0} \tag{1}$$

where, β = the attenuation of the scanned material which is a function of subject thickness and composition, and the quality of the beam;

ω = the pixel width;

h = the slice thickness;

D_0 = the maximum skin dose at a point (generally, at the position where the scan begins);

γ = the depth dose conversion to a point of interest inside the subject; and

μ = the attenuation coefficient of the volume element.

From this relationship, a number of important observations can be made. Since $\sigma^2(\mu)$ is proportional to $1/D_0$, reducing the noise by one-half means increasing the dose by a factor of four (Mc77). Because σ^2 is proportional to $1/\omega^3$, decreasing the pixel width by one-half increases the system noise by 2.7 unless the dose is increased eight times. It can also be seen that increasing the pixel width causes not only a reduction in noise but also a decrease in patient dosage. In order to obtain low noise and high resolution pictures with CT machines of scan times less than 10 seconds, large photon fluxes must be used, therefore, significantly increasing patient exposure.

To keep patient exposures at a minimum, a number of factors must be weighed by the manufacturer and the clinician. The determination of patient dose for CT scanners is difficult to obtain especially when cne considers the variations in manufacturer and use of CT equipment. Brooks and Di Chiro (Br76) suggest three ways to reduce patient dose:

1. Filter out all photons less than 50 keV to reduce the skin dose;

2. Use only 360° rotating scanners to distribute more evenly the skin dose; and

3. Control more accurately the collimation at the source(s) and detector(s).

Methods of dose reduction utilizing improved reconstruction algorithms to reduce noise contributions and the effects of beam polychromaticity are currently being investigated (Pa76;Co77;Ch77;McD75;Spi77).

Present Dose Measurement Techniques

As eloquently phrased by Schneider, "for a CT system it is quite difficult to estimate the surface flux or exposure at each point because of the complex motion and geometry of the source" (Sc78, p. 98). Because of collimation and filtration factors the

> . . .beam incident on the surface of the patient is varying in both flux and quality from point-to-point in a single traverse. This and other features make the estimation of the flux incident on the patient difficult to calculate and extremely tedious to measure. This makes detailed dose calculations difficult, either by conventional attenuation methods or by the more sophisticated Monte Carlo techniques. . . . Even if the extensive and tedious measurements required to measure the incident flux on one machine were undertaken no assumption of generality for other machines, even of the same model, could probably be made. (Sc78, p. 98)

Although some research into developing computer programs for predicting dose distributions has been undertaken (Co77;Mc75), "it seems that the only viable means of obtaining information on internal doses from CT systems is by the experimental measurement of the doses themselves" (Sc78, p. 99). In this regard, some dosimetric quantitites must be defined.

The characteristics of the x-ray beam and collimator used in a particular scanner are important in assessing the exposures expected. Most machines use a single x-ray source that is collimated (at the source and detector) to produce one or more beams depending on the generation

(i.e., translate-rotate or only rotate) of the machine in question.
Whatever the type of scanner, during an actual clinical examination, a
series of overlapping or nonoverlapping scans are made by moving the
patient couch into or out of the central beam. Thus, some terminology,
as presented by Jucius and Kambic, must be understood:

> For a single CT scan, the exposure at any location in the
> scanner area is defined as: The peak exposure at any point
> in the cross section being scanned. For a series of CT
> scans, the exposure is defined as: The average exposure to
> the central scan of a series of scans at any point in the
> volume being scanned. (Ju77, p. 2)

In reality, to effectively determine the exposure a patient is likely to
receive, a comparison of measured exposure versus image quality must be
undertaken since, if the scan is of poor quality, the clinician will order
a retake.

Dosimetric studies have been reported in the literature by both CT
manufacturers and independent researchers. The manufacturers of CT
scanner systems have provided preliminary information on the skin expo-
sures expected to be delivered to patients by their machines (Sp77;CT76;
Oh76a;Ya78;Ju77). Table 1 shows exposure characteristics of some whole
body scanners as reported by the manufacturers. Independent investiga-
tors have provided the basis (using phantoms) for dosimetric studies
correlating exposure times, pixel sizes, collimation and filtration usage,
gantry motion, and other factors with the radiation exposure that a
patient would receive (Pe73;Mc74;Mc76;Mc77;Pa76;Ba77;We77;Th78). Three
methods have been used to measure this exposure:

1. Photographic film;

2. Thermoluminescent dosimeters; and

3. Pencil ionization chambers.

Table 1

Selected Whole Body Scanner Exposure Specifications
as Reported by Manufacturers

Manufacturer	EMI	General Electric	Ohio-Nuclear
Model of Unit	5005/G	CT/T 8800	Scan 2020
Scan Motion	Translate/Rotate	Rotate	Rotate
Scan Time(s) (sec)	20;70	4.8;9.6	2;4;8;16
Slices per Scan	1	1	1
Slice Thickness(es) mm	13	5;10	4;7;10
Min. and Max. Skin Exposure (R)	0.8-3.2	5.5 max	2.4-4.6

Photographic Film

For many decades photographic film has been used to measure radiation exposures. This is done using calibration techniques that relate the density (blackness) of the film to the incident exposure (Pr64). Some advantages of film techniques include:

1. Low cost;

2. Development of an exposure profile;

3. Fast operational response;

4. Relatively large range of exposures measures; and

5. Ready availability.

Some disadvantages in using this method of dosimetry include:

1. Qualitative measurements requiring the use of densitometry for quantification;

2. Energy dependence at low energies unless filters are used;

3. Limitations to only surface measurements in CT use; and

4. Processing difficulties.

Figure 6 shows an exposure profile of a single and a series of scans that would be typically produced by a double slice scanner with contiguous incrementation between scans (Ju77). For multiple scans, as can be expected, maxima and minima will be observed whose magnitude is dependent on the separation between increments. Because of the problem of calibration for selected exposure ranges and its other disadvantages, film (except for its application as a beam localizer), is not generally considered useful in CT dosimetry.

Thermoluminescent Dosimeters

Thermoluminescent dosimeters have been used in radiation measurement applications for over two decades (Fo63). Lithium fluoride is the most commonly used thermoluminescent crystal. The advantages of TLD include:
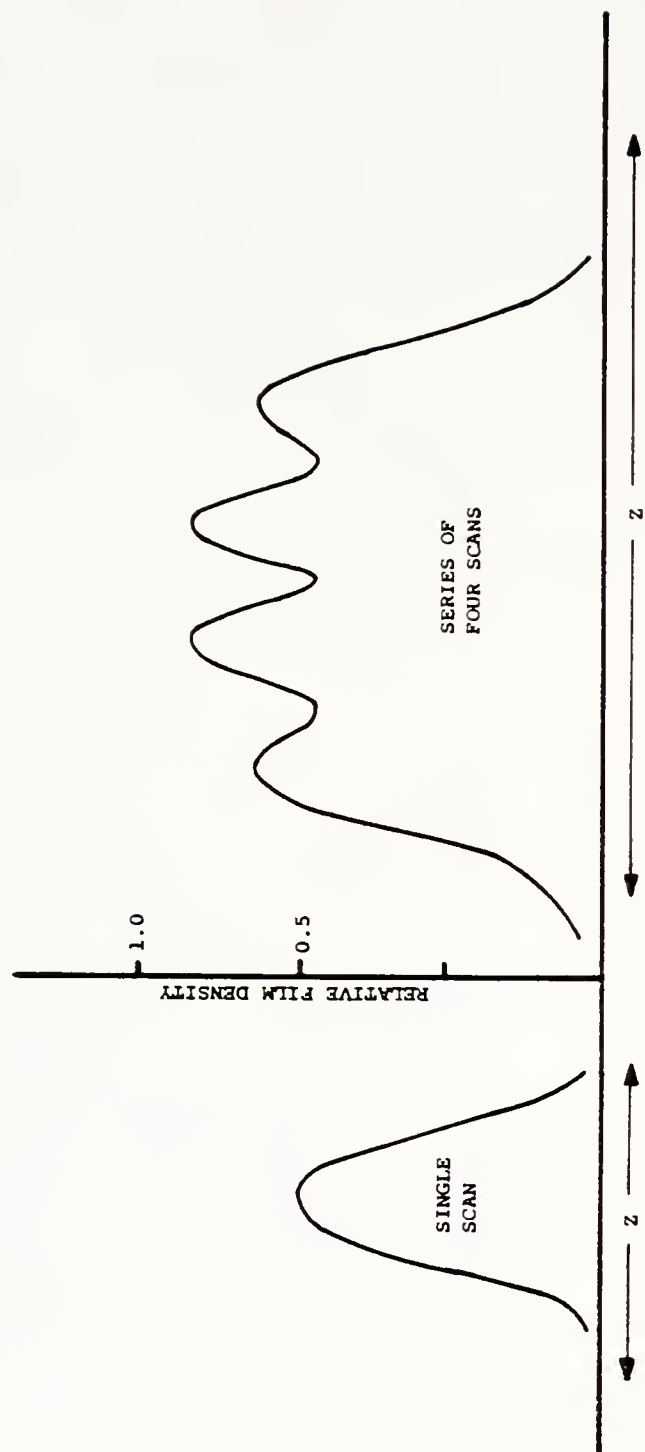
FIGURE 6. TYPICAL EXPERIMENTAL FILM EXPOSURE PROFILES (Ju77)

1. Wide range of exposure from a few mR to 10^5R;

2. Relative energy independence from 20 keV to several MeV;

3. Dose rate independence;

4. Precision as low as ±5%; and

5. Geometry approaching that of a point detector.

Some disadvantages of TLD are (TL73;Ce69;Ju77):

1. The destructive readout;

2. The need for an external means of reading the exposure;

3. The time lag between exposure and obtaining the results; and

4. The many dosimeters that are required per measurement (up to 400).

The use of TLD is the most popular method of determining exposure levels from CT scanners. Most exposure values in the literature obtained by manufacturers or independent researchers have utilized TLD singularly or in large numbers. In 1977, the BRH began using large arrays of TLD to determine exposures delivered to phantoms from CT scanners (Mor77). This investigation involved the use of a Plexiglas phantom containing 25 holes. Into each hole can be placed a Plexiglas dowel that has been hollowed-out such that 45, 3 x 3 x 1 mm chips of LiF (TLD 100), can be stacked side-by-side (Sc78). Thus, after a scan is completed, an exposure profile in the Z-direction is obtained at many locations within the phantom.

Figure 7 shows the exposure profiles of single and multiple CT scans using TLD (Ju77;Ya78). A double slice scanner with contiguous incrementation in the Z-direction is illustrated. For a single scan, the exposure to be reported is defined as the peak exposure in the scan cross section. For multiple scans, an average exposure in the central scan is desired.
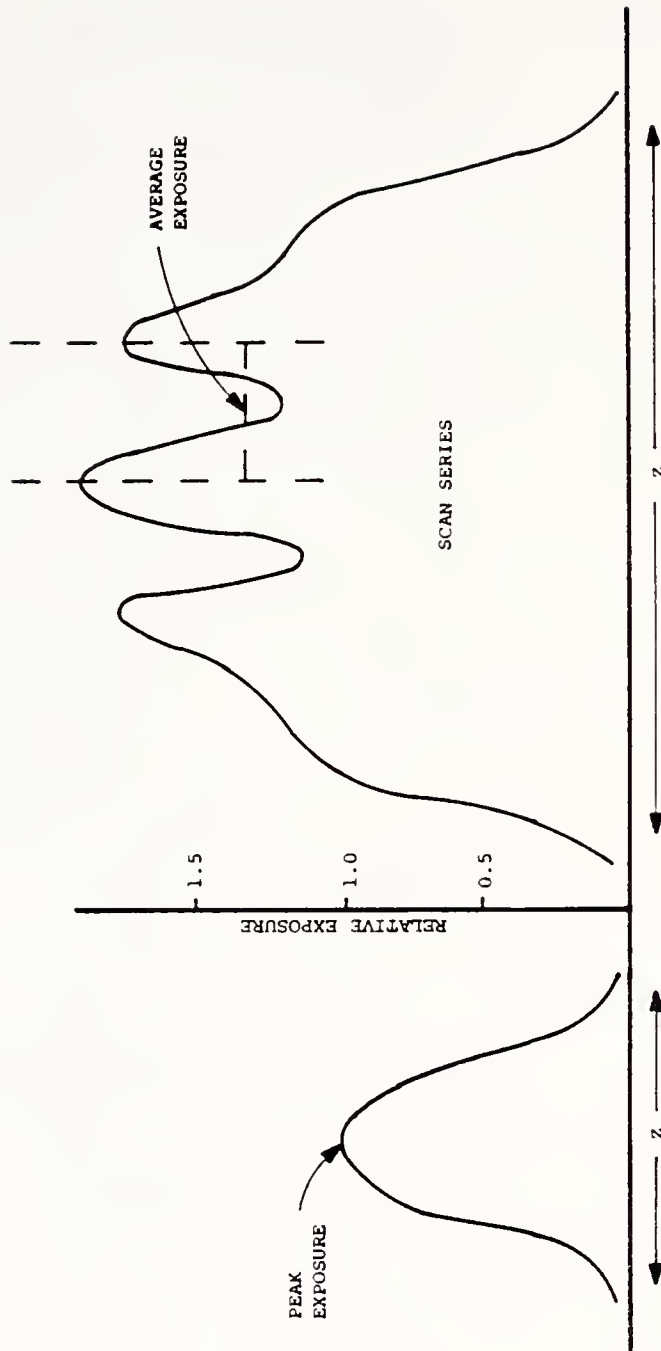
FIGURE 7. TYPICAL TLD EXPOSURE PROFILES (Ju77;Ya78)

Instead of using large numbers of TLD to obtain a Z-axis multiple scan measurement, it can be shown that all the exposure information required to report a series of scans is included in a single scan. The multiple scan profile is merely the summation of single scans that have been incremented in the normal patient couch movement distance (Z-direction). The modelling of multiple scan exposures from a single scan has proven to be advantageous (and accurate) and has shown in certain instances that the average exposure for multiple scans can be either, less than, equal to, or greater than peak single scan exposures.

The use of TLD for CT dosimetry provides high resolution dose information. The tediousness of the technique will limit its practical utilization as an "in-the-field" method of surveying CT units.

Ionization Chambers

Although ionization chambers themselves are not new, the idea of using them to measure exposures from CT units is a recent development. Ionization chambers can be designed to show (Su78;Ju77):

1. Relatively high sensitivity and large dynamic range;

2. Immediate quantitative readings; and

3. Surface or internal exposure readings.

A number of manufacturers have developed ionization chamber dosimeters that can be used for CT dosimetry (Ca77;Fa78;Vi78). Most dosimeters now available are single pencil chambers with air equivalent walls that have sensitive lengths between 5 and 10 cm. The major disadvantage of this type of chamber is that an accurate representation of a beam profile cannot be determined during a normal CT scan. However, a recent paper by Moore, et al. (Mo78) reports the development of a segmented ion chamber for CT dosimetry. This device would provide a means of obtaining

an exposure profile along the length of the chamber if minimal sensitivity
levels can be realized.

Figure 8 shows the typical response obtained from a pencil ioniza-
tion chamber due to a very narrow x-ray beam. Irradiating a small portion
of the detector is equivalent to exposing the whole chamber to a lower
intensity beam. The actual output reading of the chamber is in R-cm and
is equal to the total exposure due to primary and scatter radiation in
the Z-axis direction.

It appears that ionization chambers can be used to obtain integrated
exposure information from CT scanners. A segmented chamber would also be
able to provide an exposure profile along the length of the chamber.

Semiconductor Radiation Detectors

Most clinical dosimetry devices currently on the market use ioniza-
tion chambers, photographic film, or TLD as their x-ray detection method.
Few manufacturers have considered semiconductors for dosimetry in the
medical setting. However, with recent advances in semiconductor fabri-
cation techniques, their advantages of high speed, linear response, and
good sensitivity have increased the prospects of these devices as medical
radiation dosimeters (Si76;Th77).

Semiconductor Theory

Semiconductor radiation detectors behave like solid-state ionization
chambers (Fo63). Basically, during the process of radiation passage
through a semiconductor substance, charge carriers in the form of elec-
trons and holes are generated. When excess charges move across their
containing medium, they create an electric current due to the presence
of a modifying electric field. For a detector made of silicon, the

26
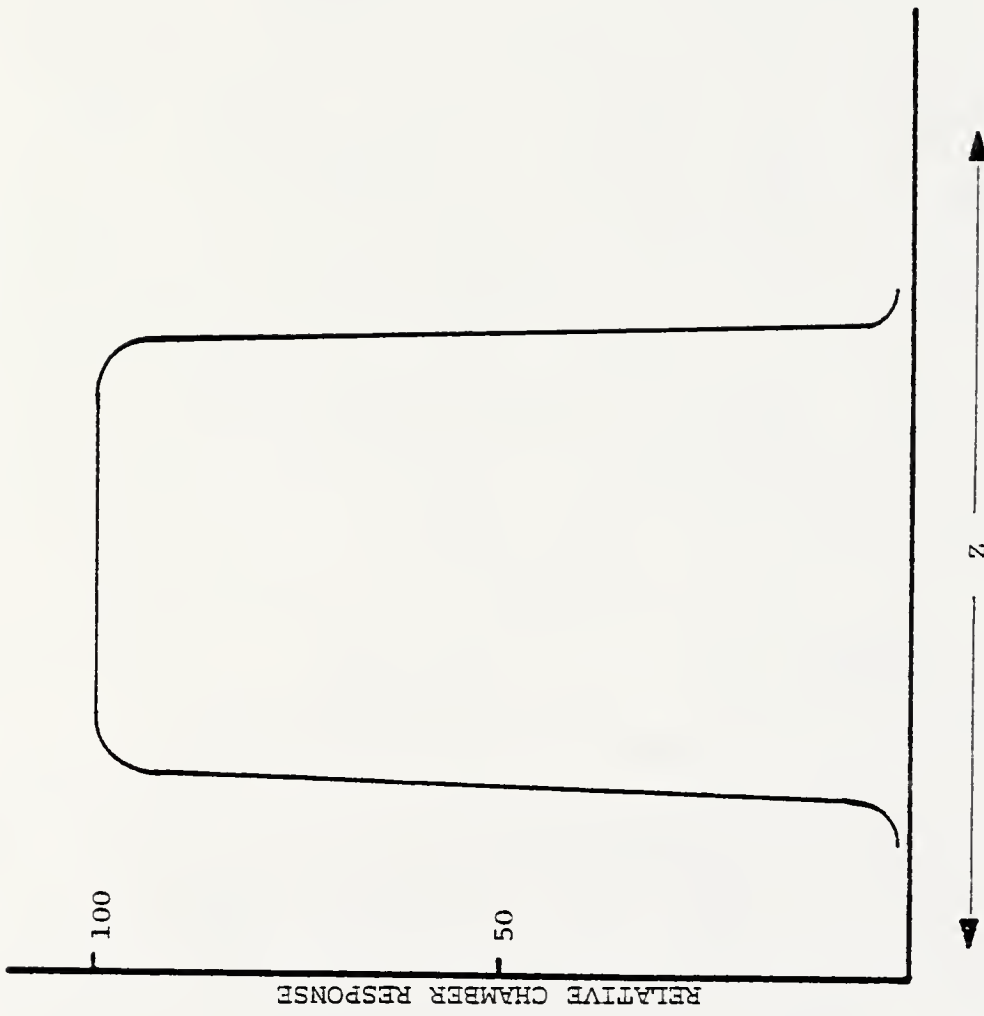
FIGURE 8. TYPICAL PENCIL IONIZATION CHAMBER PROFILE (Su78;Ju77)

minimum energy to produce an electron-hole pair (i.e., raise a valence electron to the conducting band) called the band gap energy, E_g, is 1.1 eV. However, due to energy lost in the crystal lattice from vibrational effects, the actual energy, W, required to form an electron-hole pair is 3.5 eV (Br61).

When compared to an air ionization chamber having an ion pair formation energy of about 34 eV, it can be seen that silicon has a greater radiation sensitivity by a factor of about ten. Also, since silicon is about 1850 times as dense as air, the ionization yield per unit volume is 18,500 times greater than that found in an air-filled chamber (Fo63).

For a CT machine producing x-rays with a maximum energy of 120 keV, the effective energy of the beam is about 73 keV. On either side of this value, there is a distribution of x-ray energies. The primary types of interactions occurring in the silicon crystal are due to Compton scattering and the photoelectric effect (Si76). Secondary electron production (Delta rays) also result from the primary interactions. All of these effects contribute the charge carriers that are collected to generate the output current.

The first semiconductor devices produced from silicon were of the p-n junction type. The n-type region was made of silicon in which impurity atoms with excess electrons (donor) were added. The p-type region had impurities lacking electrons (acceptor), or, in other words, having many hole sites. Due to the diffusion of charge carriers to the p- or n-sides of the crystal, a region is formed at the junction of the p-n materials in which no uncovered charges are found. This layer that is absent of free charge carriers is called the depletion or intrinsic region (Du69).

Silicon P-I-N Diodes

The size of the depletion region determines the amount of charge carrier production that will take place in the device, since for most efficient charge collection, the range of the ionizing particles should be less than the smallest dimension of the region. Another factor dependent on depletion region thickness is random noise generation. The junction capacitance is inversely proportional to the depletion width. Therefore, to keep noise as low as possible, the intrinsic width should be large (Jo62). For these reasons, silicon p-i-n diodes with thicker depletion regions than p-n junctions have been developed and applied to x-ray photon detection.

There are two major kinds of p-i-n diodes--the double diffused junction and the lithium (Li)-drifted types (as shown in Figure 9) (Bl62; Zi62;Am63;So75). For the double junction type, boron (p^+) is first diffused into a high resistivity (~2000 ohm-cm) silicon wafer. Then phosphorous (n^+) is diffused into the p^+ substrate. The width of the intrinsic region, i, is determined by the depth of the phosphorous diffusion and, of course, by the width of the wafer. The Li p-i-n is formed by the drifting of Li (n^+) under an external bias through a boron (p^+) substrate. This method produced much larger intrinsic regions, on the order of 1 mm or more, than the diffusion process. The outer electrodes of the device are made of a thin layer of either gold or aluminum.

Diode Operational Modes

There are two different modes of operation in which a silicon p-i-n diode can be configured--photodiode or photovoltaic. Photodiode operation involves the application of a reverse bias, V, to the device as shown in Figure 10. An intense electric field develops across the intrinsic
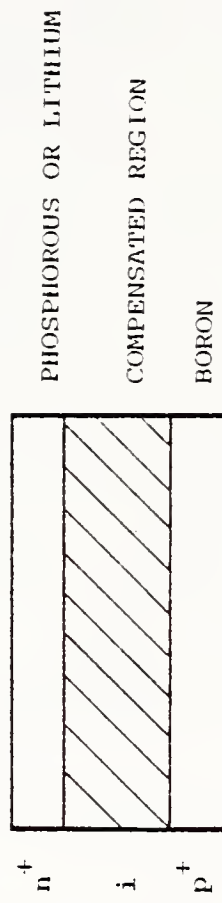
FIGURE 9. BASIC SKETCH OF A SILICON P-I-N DIODE
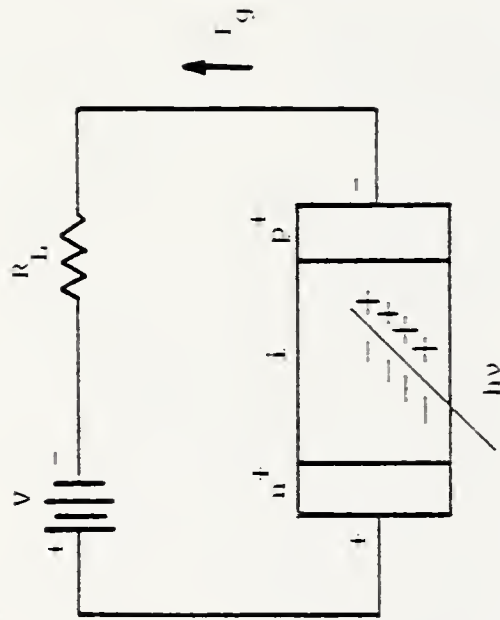
FIGURE 10. ELECTRON-HOLE PRODUCTION FROM PHOTON INTERACTIONS IN PHOTODIODE MODE OF OPERATION

region such that when an ionizing particle passes through producing elec-
tron-hole pairs, the electrons are swept toward the positive (+) elec-
trode and the holes toward the negative (-) electrode (Sc66). The genera-
ted photocurrent, Ig, is modified by a leakage current present in the
device due to the applied bias. The width of the intrinsic region and,
therefore, the sensitivity of the device are also controlled by the bias
voltage. However, increasing V also produces larger leakage currents,
thus, limiting the lowest exposure level allowable for accurate measure-
ment (Jo63).

For use as x-ray dosimeters in the photodiode mode, the p-i-n de-
vice would have to be calibrated at every applied bias voltage. This
would pose a problem in a system requiring the use of a large number of
diodes. Because the current-voltage characteristics of each device
differ, the circuitry required to apply a bias to each device so that
their outputs under the same irradiation conditions were similar, would
be formidable.

The photovoltaic mode of operation involves no externally applied
bias on the diode; therefore, the width of the depletion region remains
constant. Under equilibrium conditions, due to diffusion of charge
carriers, an electric field is generated across the depletion region
(Sc67). The field is directed from the n- to the p-type layers. When
ionizing radiation enters the depletion region, the electrons are swept
towards the n-type side while the holes move toward the p-type layer.
(Figure 11). Thus, a photocurrent, Ig, is produced consisting of the
photovoltaic output current, I_E, in the reverse direction through the
external circuit, and a junction current, I_j, in the forward direction.
For an external load resistance $R_E = 0$, the so-called short circuit DC

ELECTRIC FIELD ⟶ PRODUCED BY ELECTRON-HOLE DIFFUSION

IRRADIATION ⟵ PRODUCED ELECTRONS

IRRADIATION ⟶ PRODUCED HOLES
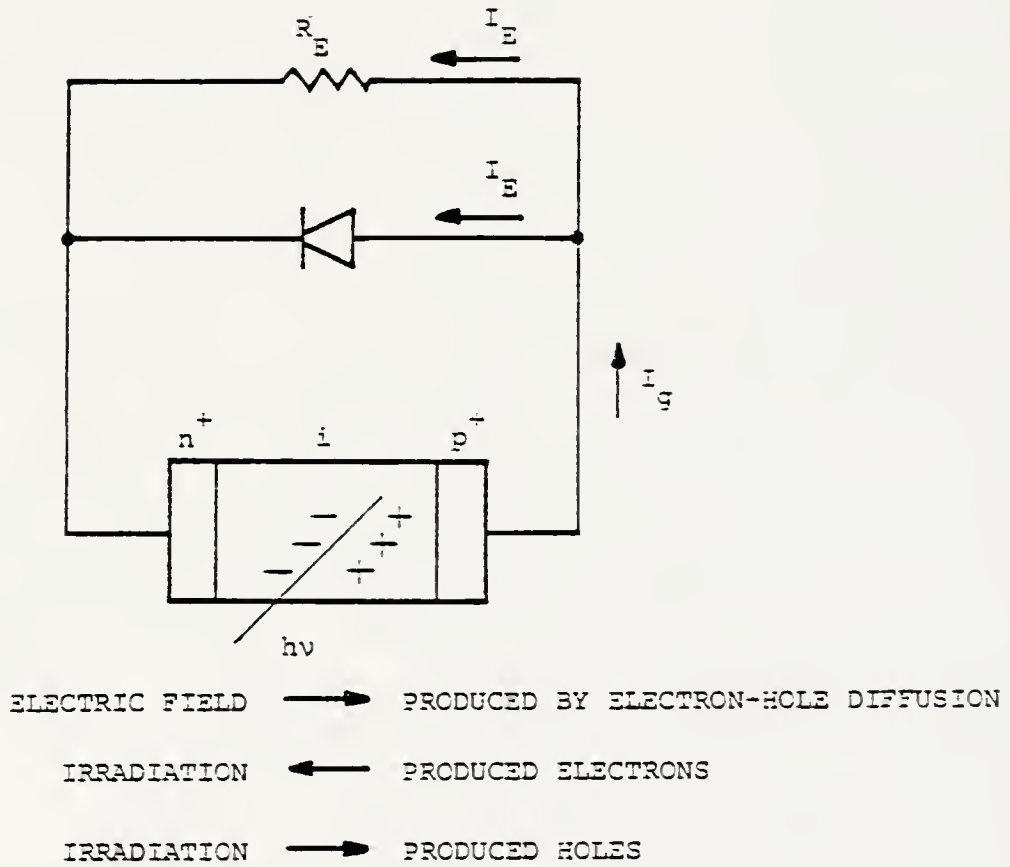
FIGURE 11. ELECTRON-HOLE MOVEMENT IN
PHOTOVOLTAIC MODE OF OPERATION

current, I_E, in the external circuit will attain its maximum value equal to I_g (Sc64).

When operated in the short circuit mode, the current, I_E, is linearly proportional to the exposure rate as seen in Figure 12. This figure shows the results of a preliminary test using an RCA C30822 silicon p-i-n diode. Practically speaking, exposure rates as low as 1.0 mR/min can be measured using silicon diodes (Ba64). Current levels in the nanoampere (10^{-9} Amp) range have been measured in diodes operated under CT exposure conditions.

The relationship between exposure and the generated current in the diode is not a simple function. According to Scharf (Sc67), the value for I_g, which under short circuit conditions becomes equal to I_E, is approximately given as:

$$I_g = I_E = \frac{q \, A \, g_o \, (w + L_n)}{(\mu L_n + 1)} \qquad (2)$$

where, q = an electron charge, coulomb;

A = the irradiated surface area, cm^2;

g_o = the generation rate of charge carriers, $cm^{-3} sec^{-1}$;

w = the width of the depletion region, cm;

L_n = the average diffusion length of electrons, cm;

μ = the linear attenuation coefficient of the radiation in silicon, cm^{-1}.

The generation rate, g_o, is related to the exposure rate as:

$$g_o = \frac{86.9 \, \mu_{en} \, (\Delta X/\Delta t)}{W(\mu_{en}/\rho)_{air}} \qquad (3)$$

where, μ_{en} = linear energy absorption coefficient of the radiation in silicon, cm^{-1};

W = average energy required to produce an electron-hole pair, 3.5 eV;
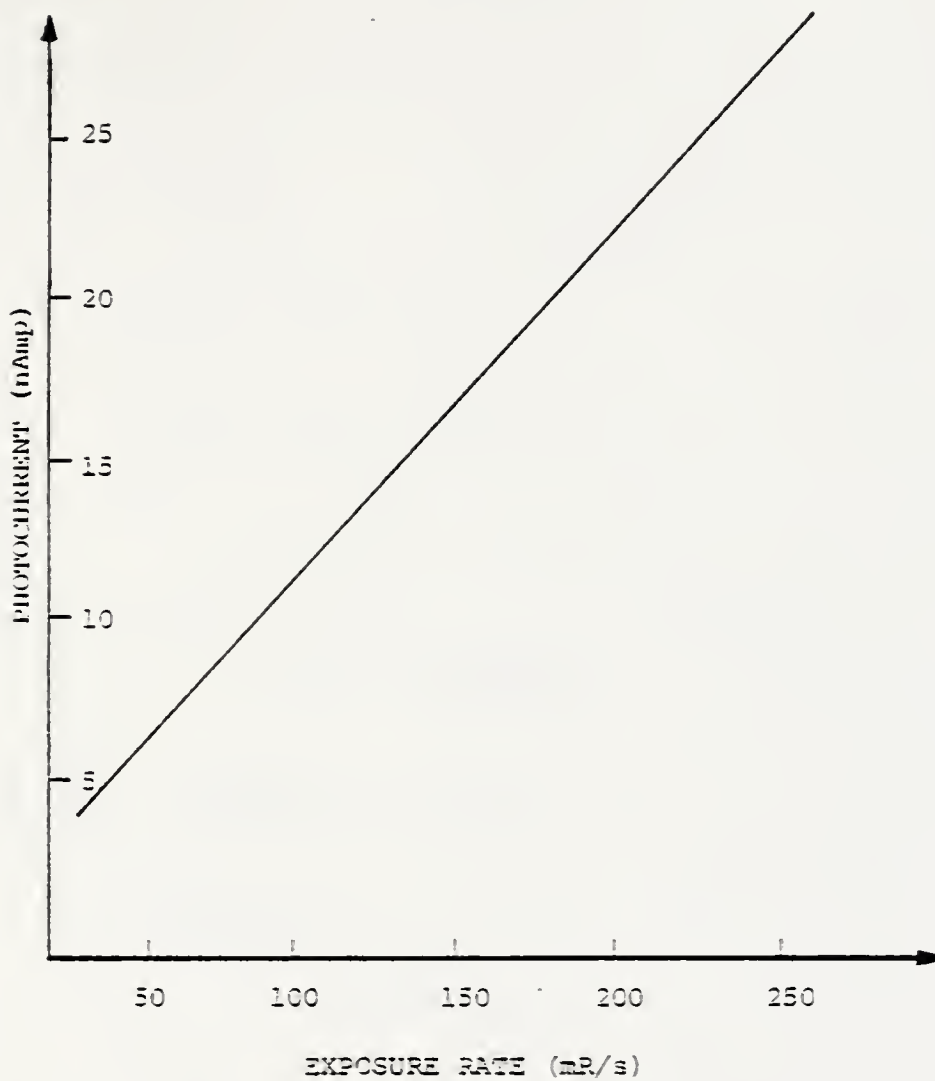
FIGURE 12.   DIODE PHOTOCURRENT VS EXPOSURE RATE FOR AN

RCA C30822 SILICON P-I-N PHOTODIODE

$(\mu_{en}/\rho)_{air}$ = the mass-energy absorption coefficient in air, cm^2g^{-1};

$\Delta X/\Delta t$ = the exposure rate, R/sec.

Rearranging equations 2 and 3 and solving for exposure rate yields:

$$\Delta X/\Delta t \ (R/sec) = \frac{I_E W (\mu_{en}/\rho)_{air} \ (\mu \ L_n + 1)}{q \ A \ 86.9 \ \mu_{en} \ (w + L_n)} \tag{4}$$

The integrated exposure, $\overline{X}$, measured by the diode is given by:

$$\overline{X} = K \ t \ (\Delta X/\Delta t) \tag{5}$$

where, K = an applied diode correction factor obtained experimentally
for each diode;

t = integration time, sec.

Diode Response Modifying Factors

Temperature effects

Temperature effects must be considered when describing the current

generated in a p-i-n diode. A current is produced in all junction de-

vices even when there is no radiation exposure (Kl73). Without an ex-

ternal bias applied, a dark current, I_T, due to the thermal generation

of charge carriers, can be measured. The magnitude, and even the sign

of this dark current, is entirely device dependent, but, generally, in-

creases with rising temperature (Kl77a). Average values for I_T are in

the 10^{-12}A range.

Variations in the ambient temperature will not affect the radiation

induced current unless the rate of electron-hole recombination is signi-

ficantly altered. Baily and Kramer (Ba64) have shown that for a p-i-n

diode operating in a temperature range from 0 - 52.5°C there is a complete

independence of generated current and temperature.

Any variations in the short circuit current, I_E, by temperature are

due directly to changes in the thermally generated current, I_T (Jo63;Sc64;

Sc71;Pet73;Kl73;Kl77a;Kl77b;Kl77c;Kl78;Ba64). This effect is related to

variations with temperature in the internal resistance of the p-i-n

junction, R_j. Figure 13 shows a diagram of the diode model as it is

connected to an amplifier circuit (K173). For short circuit operation,

the load resistance R_E equals zero and, therefore, $I_D = I_E$. However,

to measure the detector current, an instrument with a finite input

resistance must be attached in the external circuit. Assuming a value

for $R_E = 0$, I_E may be calculated from (K173):

$$I_E = I_D - I_j = I_D \frac{R_j}{R_j + R_E} .$$

(6)

The current in the external circuit, I_E, is always less than I_D because

of the presence of R_j. This means that the circuit is really not operat-

ing completely in the short circuit mode. To make the effect of R_j as

small as possible, R_E should have a low value. For example, if $R_j/R_E =$

1,000, the difference between I_E and I_D is 0.1%. Unfortunately, R_j does

not remain constant for varying temperatures. As the temperature changes,

R_j varies according to the relationship:

$$R_j \propto T^{-3/2} \exp(E_g/2kT)$$

(7)

where, T = the ambient temperature;

   E_g = the band gap energy for silicon;

   k = the Boltzman constant.

The differences in R_j observed between detectors is due to the resistiv-

ity of the silicon used in their fabrication (K173).

Appropriate values of R_E can be used under certain conditions to

compensate for the temperature effects on I_E (Sc71). In junction devices,

the sign of the temperature coefficient for the photocurrent will limit

their ability to be compensated. If a positive temperature coefficient
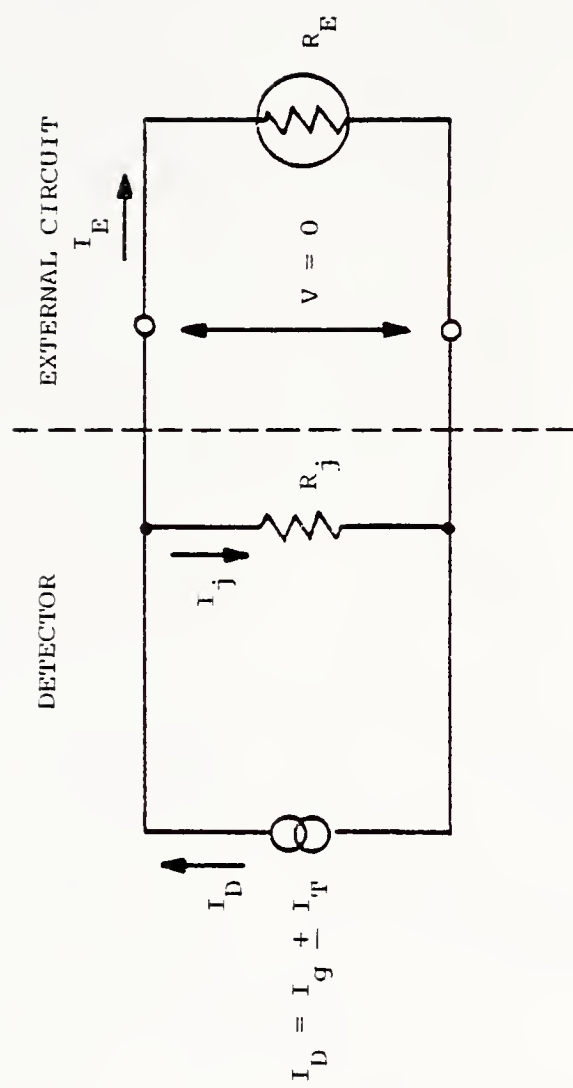
FIGURE 13. MODEL OF DIODE CURRENT MEASURING CIRCUIT (K173)

is found (experimentally), compensation can be accomplished simply by
the addition of an external load resistance, R_E, of appropriate value.
The magnitude of R_E can be found experimentally or mathematically, using
ratios of output currents (Kl78). Should the diode possess a negative
photocurrent temperature coefficient, a thermistor-type device may be
needed for compensation (Sc71).

CT scanners must be operated at temperatures between 20-25°C due
to the sensitive electronics used in their control systems. The device
to be discussed in Chapter 3 would be operated in the same temperature
environment as the scanner. Because of the characteristics of the diodes
used and the method of signal amplification employed, temperature varia-
tions will have a negligible effect on the performance of the CT dosimetry
system.

Directional dependence

A number of authors have researched the directional dependence of
silicon diodes (Wh63;Gu62;Jo62;Sh78).   It should be clear that the
geometry characteristics of each diode will dictate its directional sensi-
tivity to radiation. If a diode is operated such that the majority of
the primary beam flux is perpendicular (axial orientation) to the intrin-
sic region, as shown in Figure 14, directional dependence will be minimal.
This is shown in Figure 15 in which an RCA C30822 diode was irradiated
during preliminary testing by the author. In these tests, the diode was
located in a Plexiglas rod that was inserted into a Plexiglas phantom.
Because of the Plexiglas, scattered primary and secondary electrons
generated in the medium (assuming electron equilibrium) will also impinge
upon the detector producing interactions that add to the total number of
charge carriers collected (Ba65). Thus, the actual current I_E found in

PRIMARY BEAM
SCATTER
COMPONENT

PRIMARY
INCIDENT
X–RADIATION

SECONDARY
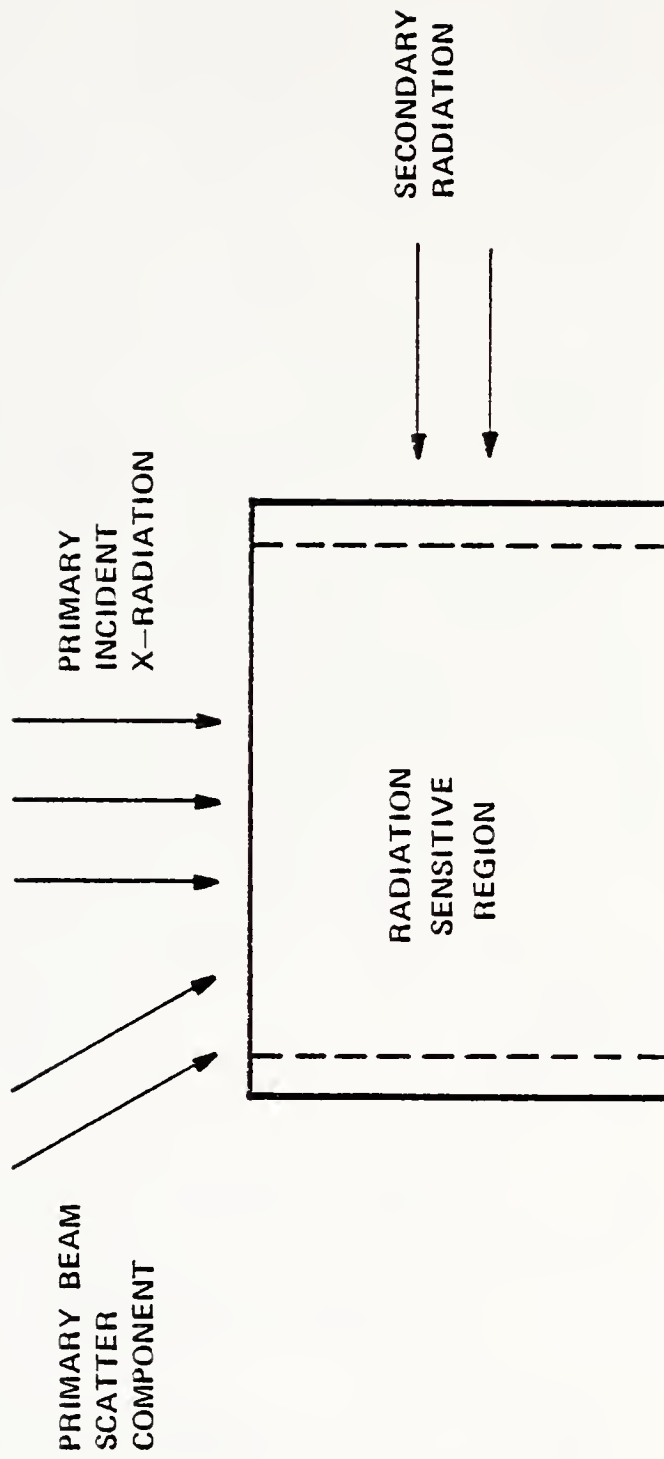RADIATION

RADIATION
SENSITIVE
REGION

FIGURE 14.   RADIATION INCIDENT ON THE DIODE
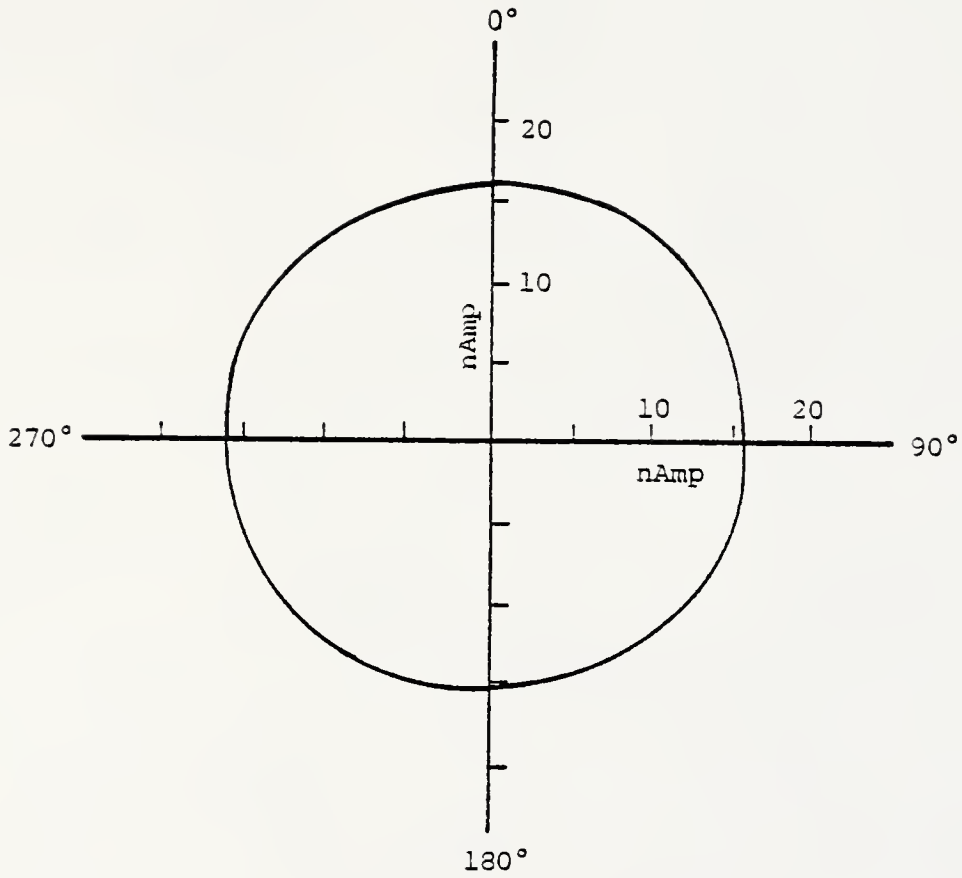
FIGURE 15. DIRECTIONAL EXPOSURE MEASUREMENTS ON THE RCA C30822 PHOTODIODE

the external circuit is due to a combination of sources and mathematical calculation for the exact photocurrent produced is difficult.

Energy dependence

Numerous investigators have demonstrated the energy dependence of the response (compared to air) of silicon diodes to the incident radiation (Sc64;Ra66;Ba64). Preliminary experimental work has indicated an increase in generated photocurrent response, shown in Figure 16, for an RCA C30822 as the energy of the x-ray beam was increased. A correction factor will probably be needed when different CT scanner energies are used.

Another aspect of energy dependence involves the use of silicon with an atomic number of 14 to measure the exposure in muscle tissue which has an effective atomic number of 7.72 (Mc75). Fowler (Fo66) states that there is increased response in silicon to the exposure rate as compared with tissue. The use of Plexiglas, with an effective atomic number of 6.47 to model tissue in the phantom should not greatly affect the number of Compton and photoelectric interactions since the electron densities of tissue and Plexiglas are similar (Ph75a;Ph75b).

Radiation damage

Silicon p-i-n diodes are subject to damage from interactions with x-rays. Damage to silicon is caused by the radiation displacing atoms from equilibrium locations producing lattice defects which serve as trapping centers for charge carriers (holes and electrons) (De64). Reported effects of these imperfections called Frenkel defects include a decrease in charge-carrier lifetime, an increase in detector resistivity, and an increase in charge-carrier generation from a trapping center (Pr64;Ro62). Coleman and Rodgers (Co64) suggest that because of their
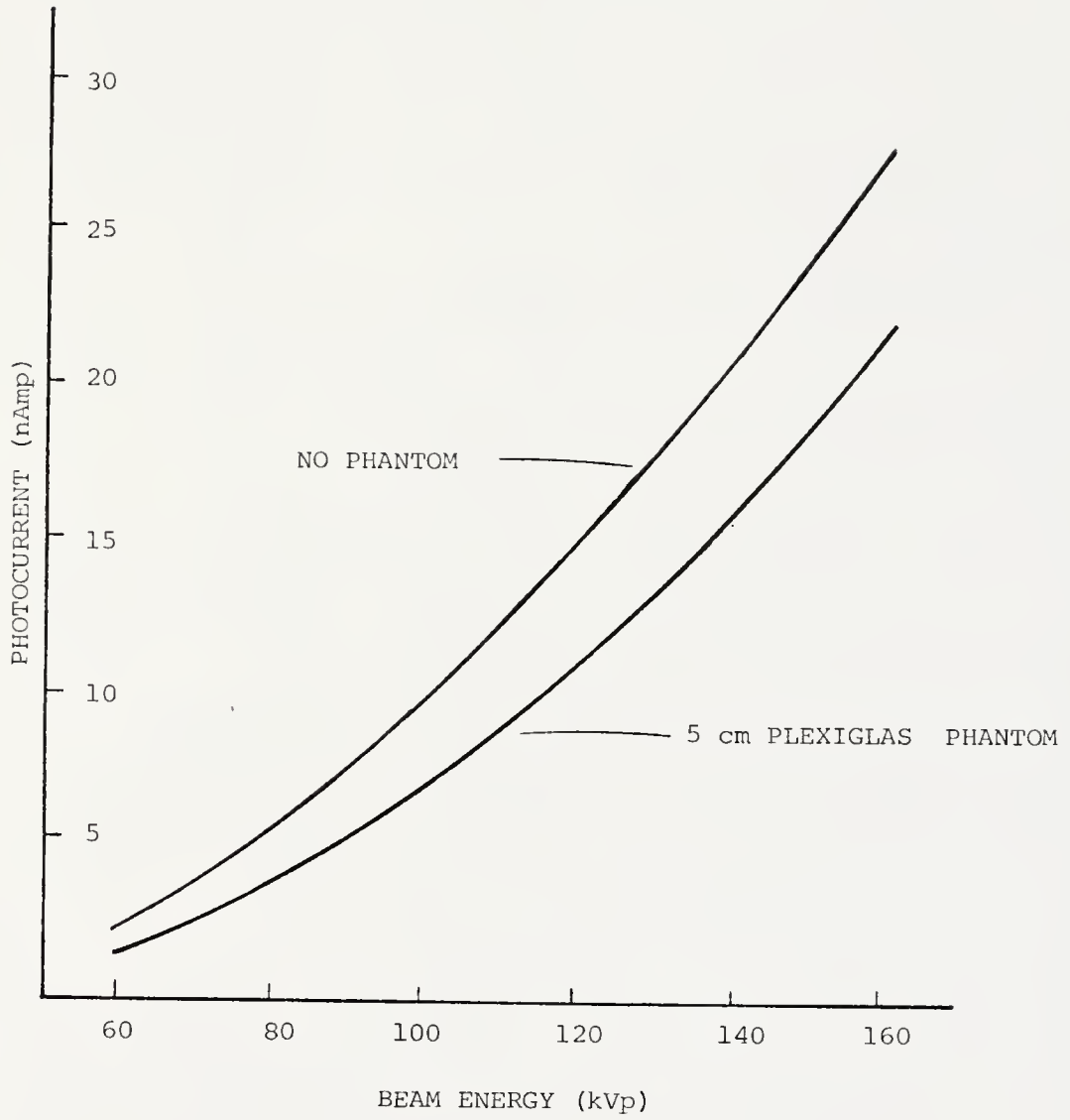
FIGURE 16.   ENERGY RESPONSE OF RCA C30822 PHOTODIODE

larger intrinsic regions, p-i-n detectors should show a larger radiation effect than p-n diodes. Loferski and Rappaport (Lo58) report no changes in short circuit currents when p-n junctions were exposed to 140 keV electrons. Raja (Ra66) indicates no observable radiation damage was exhibited by a p-n device exposed to 50 kVp x-rays for an integrated total of two million Roentgens. The probability of sustaining substantive radiation damage to the diodes used in the CT dosimeter are negligible because of the low photon energies used and since the integrated exposures are not large over the expected lifetime of the diode detectors.

Electromagnetic interference

P-i-n diodes are high impedance devices that are subject to noise generation because of electromagnetic disturbances. The diodes are sensitive to visible light and radio frequencies prevalent in buildings from power lines and other electrical and electronic equipment can cause the generation of spurious signals. To circumvent this effect, a layer of Teflon-backed adhesive aluminum foil surrounds the diode probe module. The aluminum layer is connected to the common system ground.

CHAPTER III
SYSTEM DESIGN AND CONSTRUCTION

The dosimetry system consists of two major subassemblies that form
a completely portable instrument. The block diagram in Figure 17 shows
the electronic interconnections of the system components. The diode
probe is comprised of 25 silicon semiconductor diodes which when placed
into a phantom and properly calibrated can provide accurate X-Y as well
as Z-axis directional exposure measurements. The diodes are operated
without applied bias in the short-circuit DC mode. Contiguous with the
diode probe is a suitably shielded enclosure containing the amplifying
and switching electronics for each detector.

Located at a distance of 20 feet from the Diode Probe/Amplifier
module is the Control/Readout subassembly. The control electronics will
convert the analog amplifier signal into a digital form for subsequent
analysis. The readout mechanism will consist of a thermal printer pro-
viding permanent exposure value storage from each detector as well as
positional identification information.

During a CT x-ray exposure, the photocurrent produced in each diode
is amplified and the signal is sent to the Control/Readout module. An
electrometer operational amplifier acting as a current-to-voltage conver-
ter is used for this purpose. In the Control/Readout subassembly, the
voltage signal is then converted to a square wave of a frequency dependent
on the absolute value of the input voltage. The output pulses are then
integrated in a four decade counter and their total is proportional to
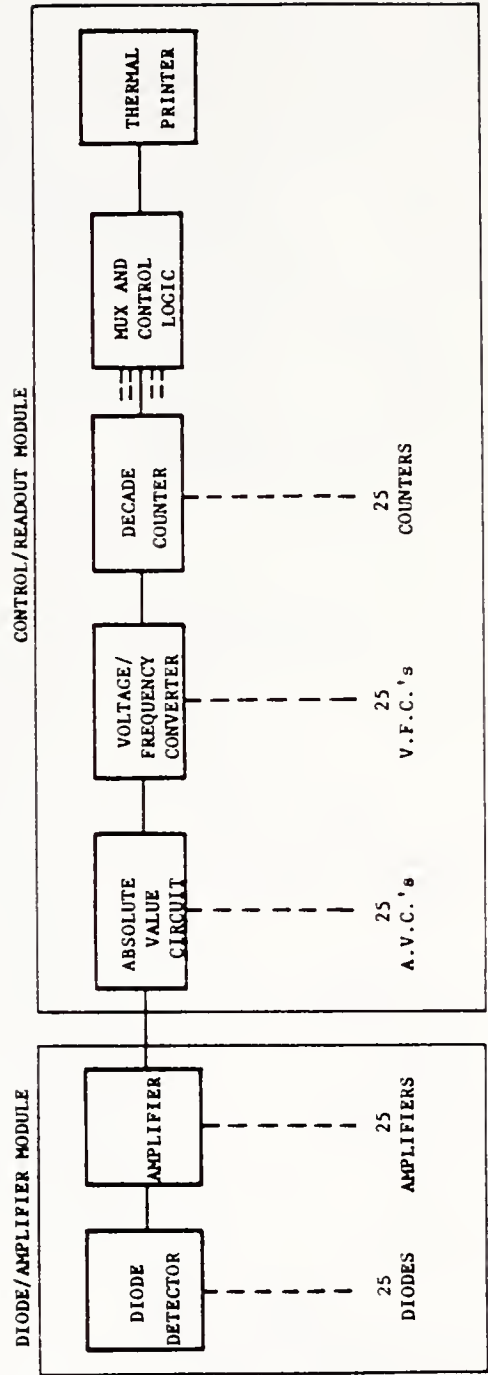
FIGURE 17. DOSIMETER SYSTEM OPERATIONAL DIAGRAM

the exposure received by the diode detector during the CT scan. Follow-
ing the exposure, an automatic dark current subtract is performed. When
readout is desired, a numerical output can be obtained using the thermal
printer.

Diode Probe/Amplifier Module

The Diode Probe/Amplifier module as shown in Figure 18 consists of
the diode probe containing 25 silicon p-i-n diodes and an enclosure hous-
ing the necessary amplifying and switching electronics for each diode.

Diode Probe

The diode probe houses the 25 diodes used as the radiation detectors.
A number of different diodes were tested in this capacity but the RCA
C30822 was chosen because of its small size (5 mm diameter active region),
large cross-sectional area ($20mm^2$ active area), and high photocurrent
output. The C30822 has an n-type substrate that is diffused with boron
to form the intrinsic region. This depletion region is between 100 and
150 µm in depth. Experimental values for the C30822 showing the direc-
tional dependence, photocurrent vs. exposure rate, and energy dependence
were presented in Chapter 2. Further tests with other diodes of the
same type showed these values to be similar for the group used in the
probe.

A unique mounting arrangement has been developed to house the detec-
tors positioned in the probe. Figure 19 shows a cross-sectional view
through the diode probe and Figure 20 is a photograph of the completed
assembly with the diodes emplaced. The probe consists of a section of
12.7 mm diameter Plexiglass rod stock that has been milled as depicted
in Figure 19 by Metal Fab, Inc. (Gainesville, Fla.). The rod was
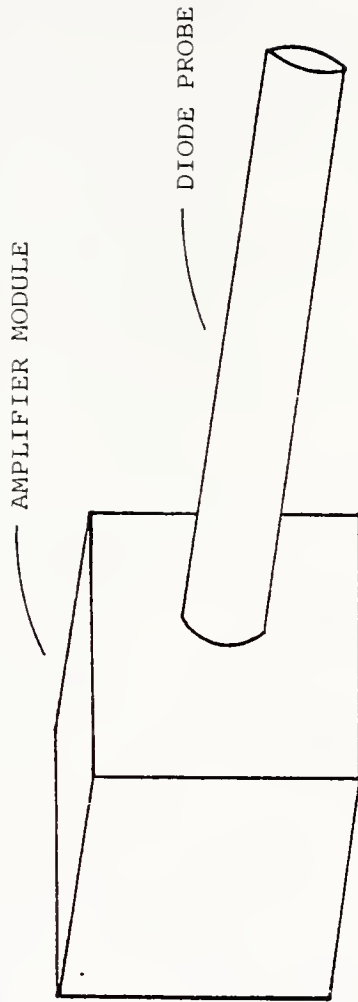
FIGURE 18.   DIODE PROBE/AMPLIFIER MODULE
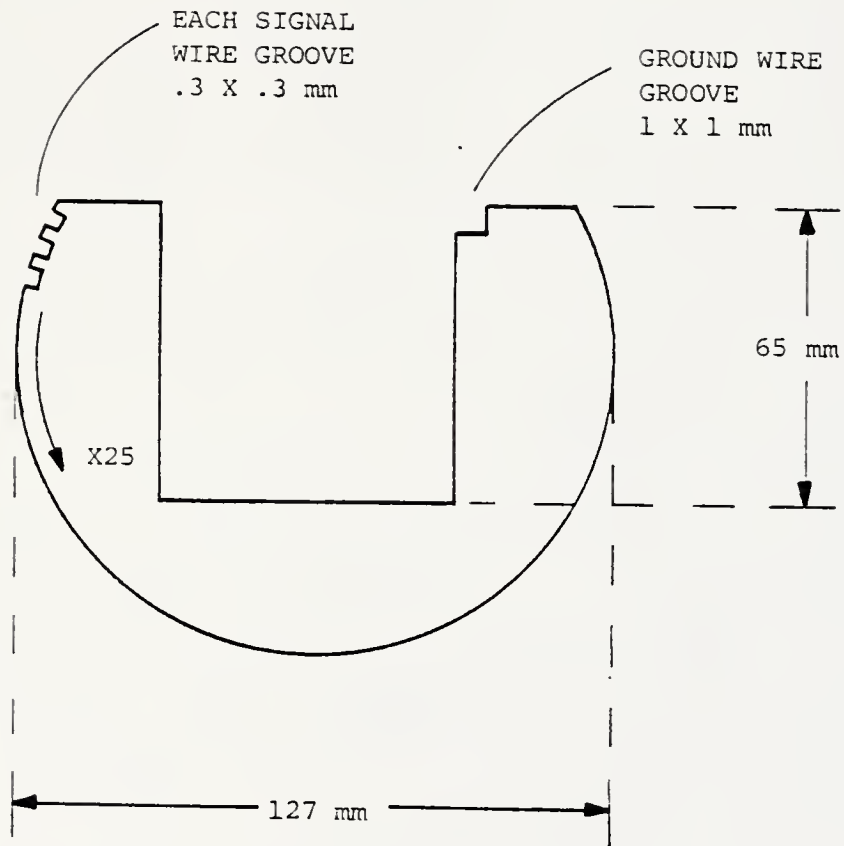
FIGURE 19.   CROSS-SECTIONAL VIEW OF
            PLEXIGLAS DIODE PROBE

FIGURE 20. DIODE PROBE ASSEMBLY
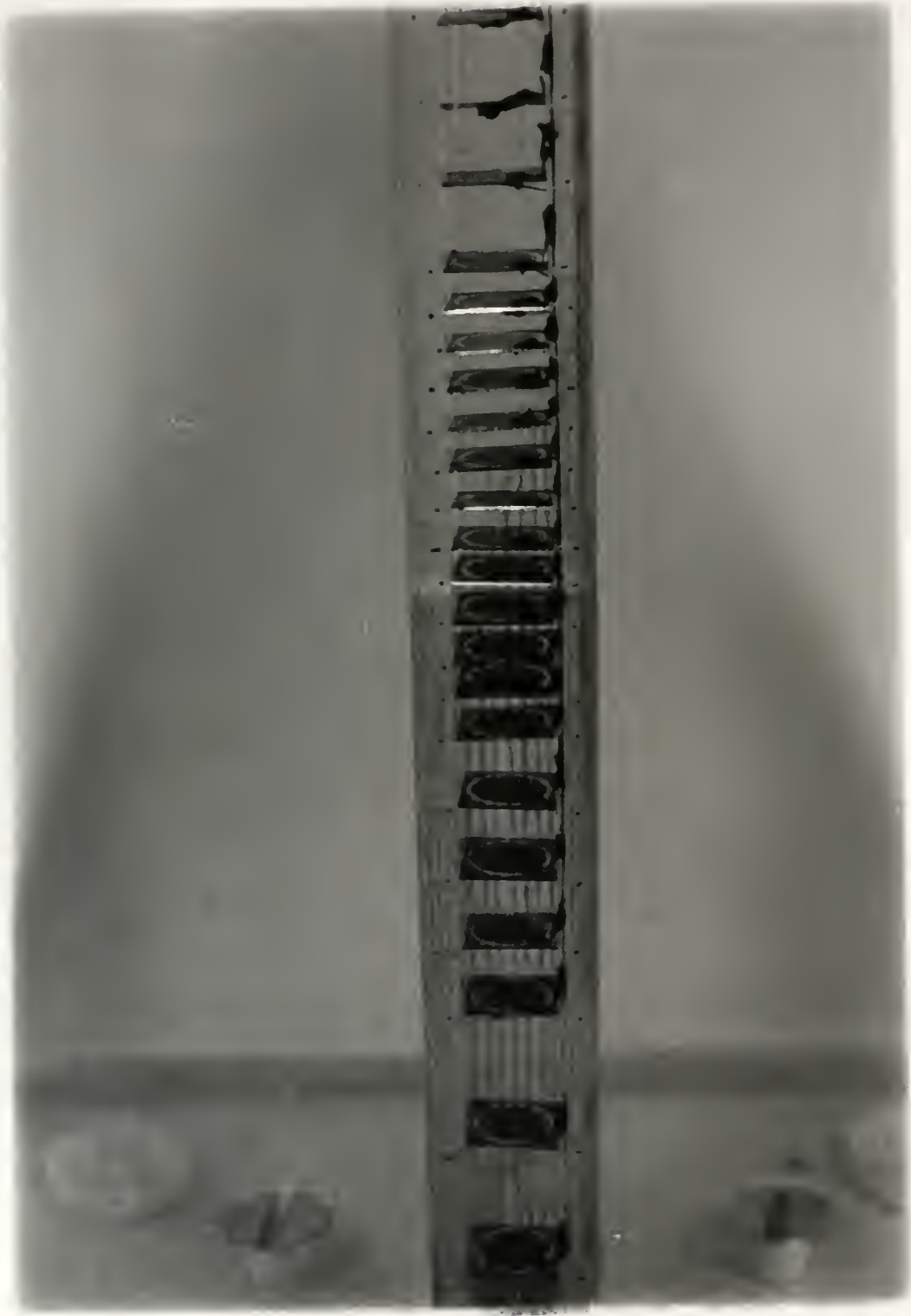
designed to allow the portion extending from the amplifier enclosure to be placed into a 125 mm thick plexiglass test phantom for radiation measurement purposes. Inside the amplifier module, the probe extends to the output socket connector.

As seen in Figure 19, a portion of the circumference of the rod was milled off and then 25 equally spaced grooves running longitudinally along the major axis were cut into the remaining circumference of the rod. Into the center of the previously machined top portion, a deep groove 120 mm in length was milled. It is into the center of this groove that the 25 diodes were placed with the separation between devices shown in Figure 21 for one-half of the symmetrical array. Into each groove on the outer circumference of the rod, a hole was drilled at a point 1 mm to one side of the position of the diode placement. This was done to allow signal wires to be brought from the n-side of each diode to the amplifier module. An additional groove also has been milled parallel to the deep center groove along the entire length of the rod to accommodate a wire carrying the common ground return from the p-side of each diode.

Because its low atomic number would minimally perturb the x-ray flux, aluminum wire 0.008 inch thick (EC-soft) was obtained from the California Finewire Corp. (Grover City, Calif.) to carry the current signals from each diode. The aluminum wire was attached to each diode using a carbon-based epoxy Eccobond 60-L obtained from Emerson & Cuming, Inc. (Canton, Mass.). This carbon epoxy was chosen because it contributed negligibly to the scatter radiation generated in the probe. Following diode emplacement and wiring, a silicone potting compound Eccosil 2CN (Emerson & Cuming, Inc.) was used to encapsulate the detectors to exclude the presence of air in the probe.
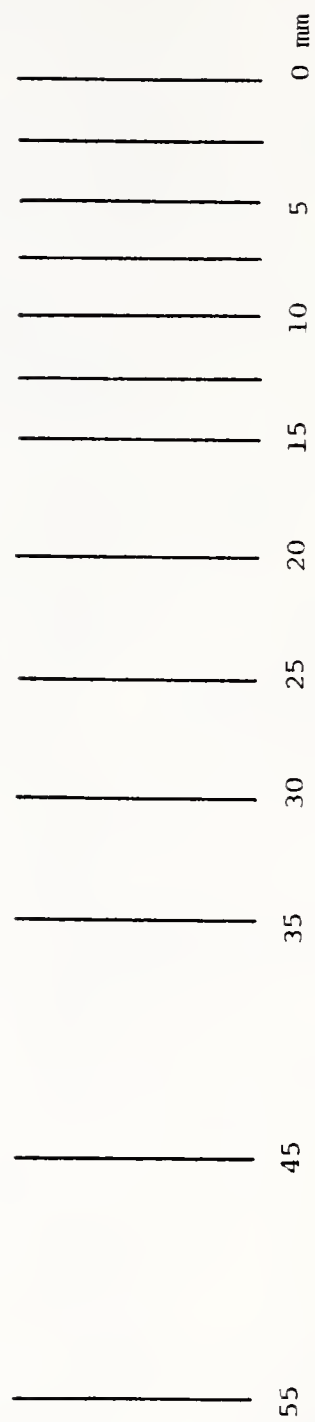
FIGURE 21. DIODE SPACING IN THE PROBE FOR ONE-HALF
OF THE SYMMETRICAL ARRAY

To complete the probe, a Plexiglas top section was milled that closely replaced the original portion that was previously removed. Two layers of a Teflon-coated aluminum foil were then folded around the probe and connected to the system ground. Finally, the entire portion of the probe not placed into the amplifier module was inserted into a section of 19 mm diameter Plexiglas tubing that provided structural strength and environmental protection.

Amplifier Module

The amplifier module is directly connected to the diode probe. A portion of the probe extends into the module and is used as a guide for the output wires from each diode. The amplifier enclosure is a square box 100 mm on a side and is made of .063 inch aluminum sheet. Figure 22 shows the general layout of the amplifier module. The three printed circuit boards containing the amplifier electronics are visible. The socket at the rear of the enclosure allows output of the amplified signals from each detector and input of power and switching control signals.

Operational amplifier characteristics

An operational amplifier (op amp) is a directly coupled amplifier employing feedback to control signal gain potentials (St76). The device is constructed of many transistor amplifiers and is available in monolithic or discrete forms. The op amp can operate as an amplifier, controller, or signal generator over a wide variety of frequencies including DC operation. For its present purpose as a current-to-voltage converter, the op amp is the logical choice because of its high stability over time, temperature variations, and gain changes.

The ideal op amp possesses the following characteristics:

1. Differential voltage gain = ∞;

2. Common mode voltage gain = 0;
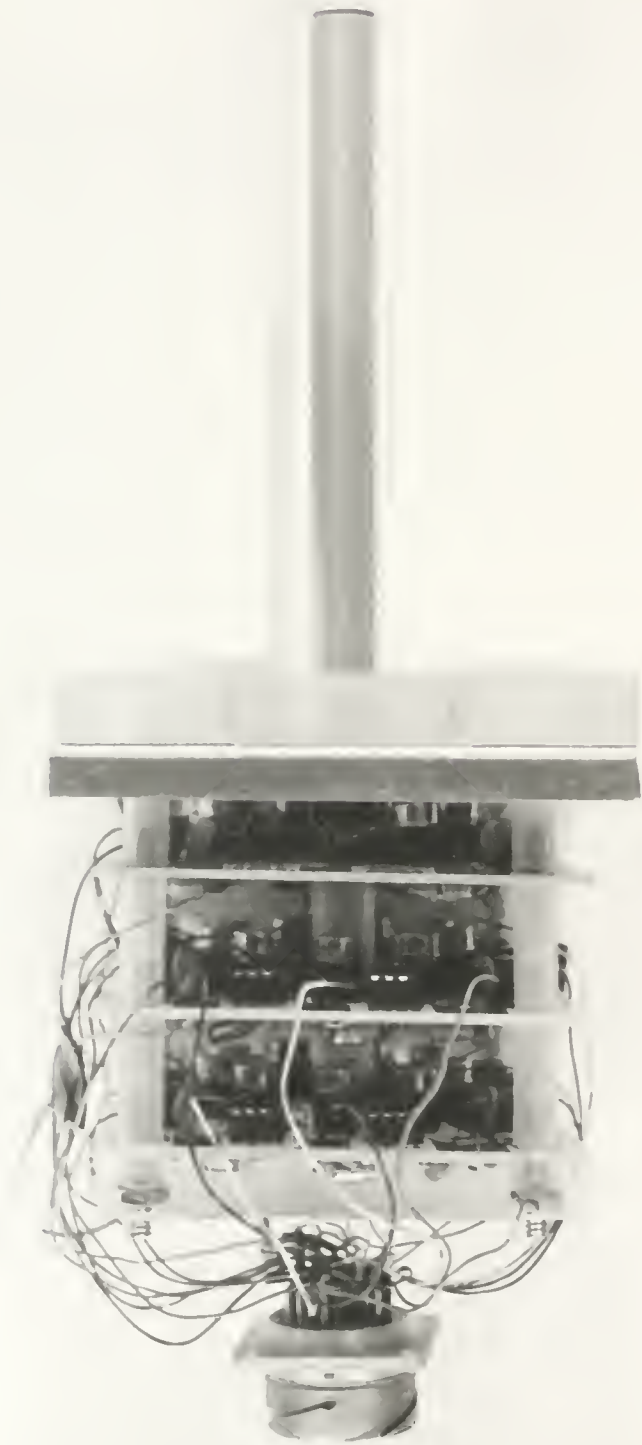
FIGURE 22. AMPLIFIER BOARD CONFIGURATION

3. Bandwith = ∞;

4. Input resistance, R_i = ∞;

5. Output resistance, R_o = 0;

6. Perfect balance, output voltage V_o = 0, when input voltage, V_i = 0;

7. No parameter drift with temperature changes; and

8. Input noise = 0.

None of these ideal parameters could or even need be obtained in actual practice. For the purposes of the amplifier in this project, compromises can be made so that only a few of these characteristics need to approach the ideal.

Op amp operating configurations

There are two basic configurations in which an op amp, using feedback, can be described--the noninverting and inverting modes. A brief description of the noninverting mode will be given followed by an analysis of the inverting-type since it will be used for the amplification in the dosimeter.

The noninverting op amp (Figure 23) uses the noninverting lead (+) for signal input and the inverting connection (-) for feedback purposes. The output voltage, V_o, in this circuit is in phase with the input voltage, V_i. This configuration has many important applications including its use as a voltage follower allowing for isolation of signal source and load (Gr71).

The inverting configuration (Figure 24) requires the input signal to be fed into the inverting (-) input while the noninverting input (+) is connected to common signal ground. There are two basic operating rules (ideally) for this setup that simplify circuit analysis. First, the two op amp input terminals draw no bias current. Secondly, the voltage between the input terminals, V_x, equals zero (virtual ground). From this
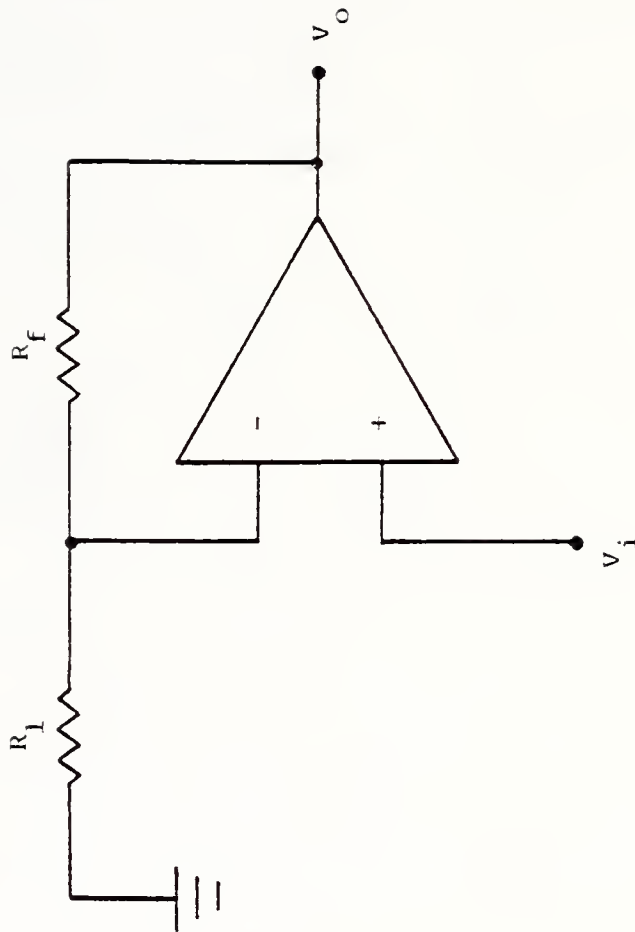
FIGURE 23. NONINVERTING OP AMP CONFIGURATION
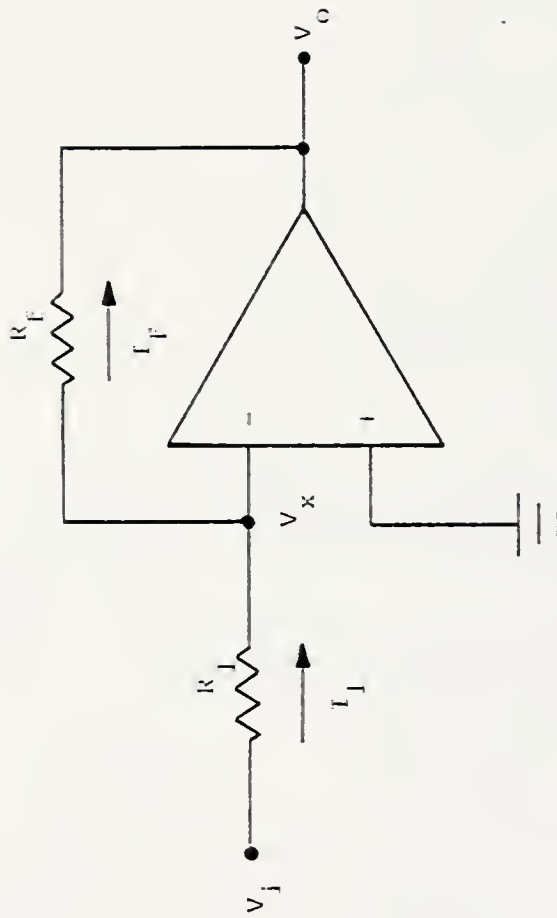
FIGURE 24.   INVERTING OP AMP CONFIGURATION

it should be realized that the current flowing through R_1 is I_1 and is numerically equal to $(V_i - V_x)/R_1$. The current flowing through R_f is equal to $(V_x - V_o)/R_f$. Since the inverting input has infinite input resistance and ideally draws no bias current, all of I_1 must pass through R_f. Therefore, $I_1 = I_f$, and since $V_x = 0$,

$$I_1 = \frac{V_i}{R_1} = - \frac{V_o}{R_f} = I_f, \text{ and,} \tag{8}$$

$$V_o = - I_1 R_f . \tag{9}$$

Op amp error factors

There are a number of factors that could influence the operation of the amplifier in this circuit. Ideally, these parameters would not exist, but in the real world they can produce errors and, consequently, their presence must be known and then minimized. Op amp designs are continually being improved leading to more ideal devices.

Input offset voltage (V_{os}). When the input voltage, V_i, to an op amp is zero, ideally its output is also equal to zero. In most cases, however, a finite output voltage can be measured even when the input is zero. The input offset voltage is that potential applied to bring $V_o = 0$. The value of V_{os} is temperature sensitive and is usually defined in relationship to temperature (i.e., $\mu V/°C$).

Input bias current (I_b). The input bias current, I_b, is the average of the two op amp input currents. Ideally, $I_b = 0$, so that possible interferences with the feedback circuitry are removed. The I_b of the op amp should be minimal since this, together with noise properties intrinsic to the device, determines the lower limit of current measurements.

Input offset current (I_{io}). The input offset current, I_{io}, is the numerical difference between the currents going into both inputs of the op amp. This parameter is a function of temperature so circuit component compromises must be made for operation in the temperature range of interest (Mi72).

Slew rate. The slew rate of an op amp describes the amplifiers ability to change its output voltage when a step input voltage is applied. This rate of change is usually given in volts per microsecond (V/µs).

Circuit description of the amplifier module

Figure 25 shows the amplifier circuit that is used for each of 25 diodes in the dosimeter. A number of op amps were tested but the Analog Devices, Inc. (Norwood, Mass.) AD 515LH was chosen for this application. The AD 515LH exhibits a low input bias current of 75 femtoamp maximum, a typical input offset voltage of 0.4 mV, an offset voltage drift of only 25 µV/°C, and a slew rate of 1.0V/µs (An78a).

The amplifying circuit is designed to function as an exposure rate measuring device. When used to monitor the radiation output of CT scanners, this operational mode causes some problems. It is generally observed that for CT units to perform very rapid scans, a large photon flux must be emitted to obtain sufficient information in a short time period. This means that the silicon diodes will be required to measure large, almost instantaneous photon fluxes from fast scan (pulsed) machines as accurately as they would measure smaller magnitude fluxes from slower devices (continuous flux). To ensure a reasonable dynamic response in the amplifier, two input voltage ranges have been incorporated into the feedback loop. The equation that describes the operation of the current-to voltage converter is:
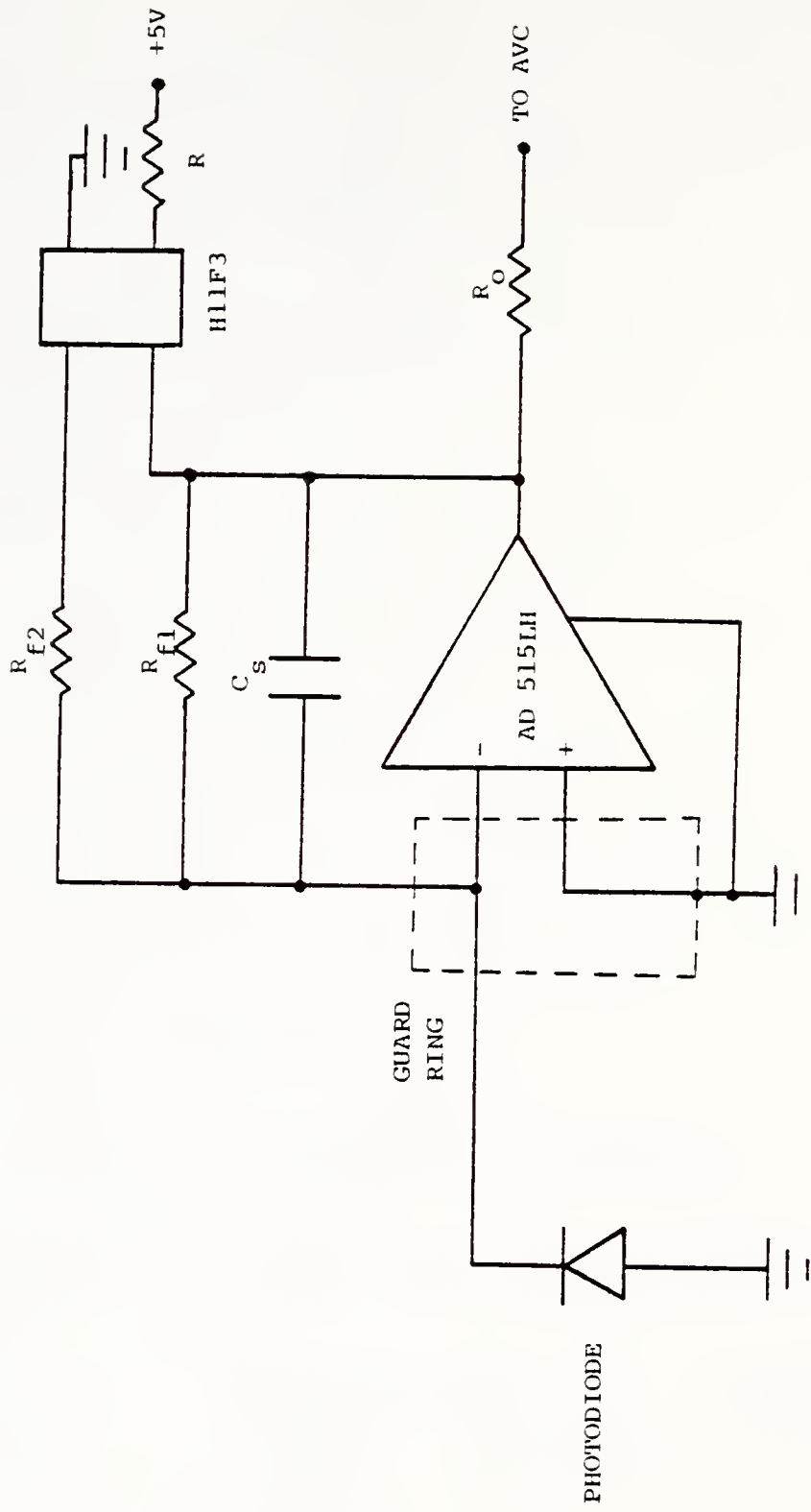
FIGURE 25. CURRENT-TO-VOLTAGE CONVERTER CIRCUIT

$$V_o = - I_D R_f \qquad (10)$$

where, V_o = the output voltage;

I_D = the diode produced current; and

R_f = the feedback resistance.

Because the amplifier is used in the inverting mode, the output voltage is the opposite polarity of the current flowing into the negative inverting input.

To facilitate these two input ranges, resistances R_{f1} and R_{f2} are located in the feedback loop. Feedback resistance R_{f1} is permanently located in the circuit and defines the lower maximum input exposure rate range which has been defined as 2 R/sec. Resistance R_{f2} which has a value fifty times less than R_{f1} is used to measure the maximum exposure rate of 100 R/sec and can be connected into the circuit using a General Electric (Syracuse, New York) H11F3 opto-isolator. The switch used to perform this function is located on the front panel of the Control/Readout module. The opto-isolator exhibits an "off" resistance measured at about $5.6 \times 10^{11}\Omega$, and an "on" value of about 300Ω thus, not affecting the operation of the circuit. Resistances R_{f1} and R_{f2} are in parallel so the effective feedback resistance when the opto-isolator is activated equals:

$$R_{eff} = \frac{R_{f1} R_{f2}}{R_{f1} + R_{f2}} . \qquad (11)$$

This effective resistance is slightly less than the value of R_{f2} but the error is not important in circuit operations.

If it is assumed that the maximum voltage output of the amplifier is 10 volts, then a calculation for the desired feedback resistance can be made. Previous experimentation with diagnostic x-ray machines

has shown an average diode current/exposure rate of about .115 namp/mR-sec. This measurement was performed using the C30822 diode located in a Plexiglas phantom at 5 cm depth (assumed average tissue depth). Using this value and rearranging equation (8), for the maximum exposure rate of 100 R/sec (10^5 mR/sec) gives the following value for R_{f2}:

$$R_{f2} = \frac{10 \text{ V}}{.115 \text{ namp/mR-sec} \times 10^{-9} \text{ amp/namp} \times 10^5 \text{mR/sec}} \quad (12)$$

$$= 8.69 \times 10^5 \Omega$$

Since the lowest exposure rate range must have a resistor 50 times as large as R_{f2}, then R_{f1} should equal $4.35 \times 10^7 \Omega$. The actual values chosen were: $R_{f1} = 5 \times 10^7 \Omega$ and R_{f2} $1 \times 10^6 \Omega$. The resistors, obtained from Eltec, Inc., (Daytona Beach, Fla.), were high precision devices (±2%) that exhibited low drift with temperature (E178).

A 5 pf polystryene capacitor, C_s, is located between the inverting input and the output terminals of the op amp. The capacitor is used to stabilize the feedback loop because of the instabilities that may arise due to the presence of a parasitic capacitance of 2-5 pf located at the inverting input of the op amp (An78a;St76).

The output of the amplifier must pass through 20 feet of shielded multi-conductor cable before the signal reaches the Control/Readout module. Because the capacitance in the cable (Belden 8776) is about 40 pf/ft, resistor R_o is located at the output signal of each amplifier to set up a time constant limiting the output current of the device.

Belden 8776 is a 15 pair individually shielded cable that is used to interconnect the dosimeter's two modules. Twenty-five conductors are used to carry the output from each amplifier. Two conductors supply ±12 volts to the AD 515LH op amps and another line is used to turn the

opto-isolators on through current limiting resistors. The shields located. on each pair of wires are connected to the common system ground. Thirty-seven pin Amphenol plugs and sockets are used between both modules to permit precise and positive transfer of signals.

All of the electronic components comprising the amplifier module are located on three identical double-sided epoxy-glass printed circuit boards. The boards were designed by the investigator but fabricated by Technetronics, Inc. (Casselberry, Fla.). Figures 26 and 27 show the component and wiring sides of the boards, respectively. Two boards contain nine separate amplifier sections while one board holds only seven amplifier circuits. Nylon integrated circuit sockets are employed for op amp emplacement. Because of the low currents to be handled by the amplifier, shielding and guarding techniques must be emphasized. Guard rings surrounding the inverting input (on both sides of the board) and tied to ground are necessary to prevent leakage current errors. Since high impedance circuits are conducive to picking up stray AC signal in the environment, the amplifier boards are completely enclosed in a grounded metal box.

The output current from the n-side of each detector is directly routed to its complementary amplifier input (inverting input). The location in the op amp socket and the printed circuit board through which the inverting lead passes has been drilled out, thus ensuring that this highly sensitive input does not come in contact with any material that could lead to the generation of noise signals in the amplifier. The feedback resistors R_{f1} and R_{f2} and stabilizing capacitor C_s are directly connected to the inverting lead. The opposite ends of R_{f1} and C_s are connected to the socket pin that contacts the output pin of the amplifier. Resistor
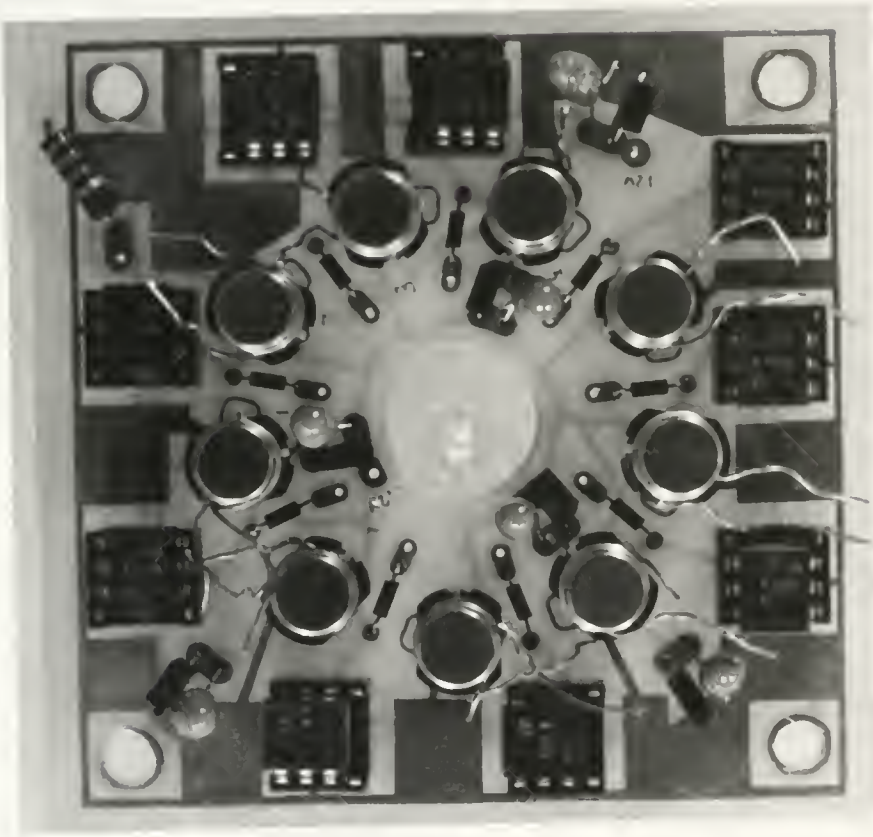
FIGURE 26. COMPONENT SIDE OF AMPLIFIER BOARD
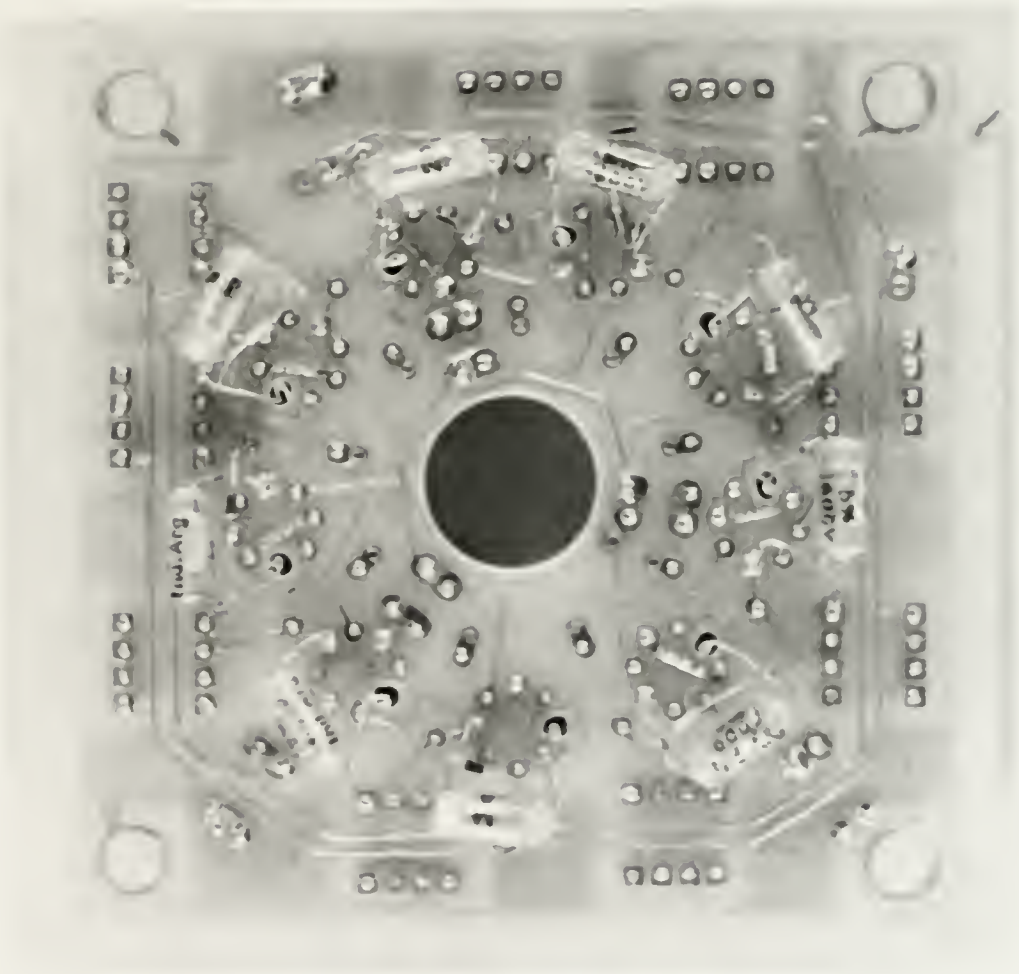
FIGURE 27. WIRING SIDE OF AMPLIFIER BOARD

R_{f2} is attached to an input of the opto-isolator for each amplifier.
The opto-isolator output is sent to the amplifier output pin. Resistor
R_o is mounted on the printed circuit board and the final output from each
amplifier is sent through it to a 37 pin socket which is located at the
rear of the amplifier module.

Power supply bypassing is used on the circuit boards to eliminate
high and low frequency noise. A 22 µf tantalum electrolytic capacitor
and a .01 µf ceramic capacitor combination is present for every three
amplifiers on the three boards.

Amplifier response

An amplifier does not instantaneously show a voltage output when an
input signal is applied. Likewise, the amplifier output does not imme-
diately drop to zero when the input signal is removed. If this were true
(an ideal amplifier), the equation describing the area under the curve in
Figure 28a would be simply:

$$\text{TOTAL AREA} = V_o\, t_o, \tag{13}$$

This represents the integral of the voltage signal V_o over time t_o and
is proportional to the x-ray exposure received by the silicon diode de-
tectors.

In the amplifier circuit described previously, a finite feedback
resistance and capacitance is present in all situations. Figure 28b
illustrates an approximation of the actual curves describing the rise and
decay exponentials of the amplifier. Modelling this curve produces two
integrals:

$$\text{AREA} = V_o\, [\int_o^{t_o} (1 - e^{-t/\tau})\, dt + \int_{to}^{\infty} e^{-t/\tau} dt] \tag{14}$$

$$= V_o\, [\, t_o - \tau + 2\tau e^{-t_o/\tau}] \tag{15}$$
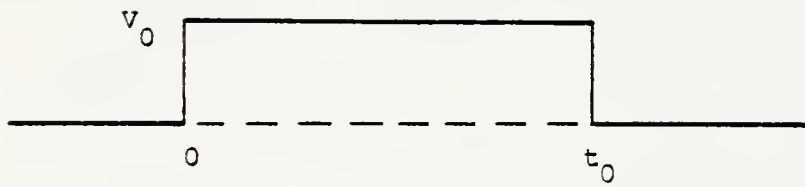
a.) IDEAL AMPLIFIER RESPONSE
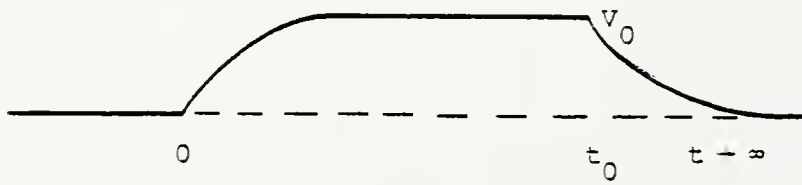
b.) REAL AMPLIFIER RESPONSE

FIGURE 28.   DIODE DETECTOR AMPLIFIER RESPONSE

In these equations, t_o is the scan time of the CT unit and τ is equal to the feedback resistance multiplied by the feedback capacitance C_s. If $C_s = 5$ pf, $R_{f1} = 50 \times 10^6 \Omega$, and the CT scan time is one second, the area under the curve from equation (14) equals .9998 V_o. This value when compared to an ideal amplifier response of 1 V_o shows only a .025% difference. If $R_{f2} = 1 \times 10^6 \Omega$, a value of the total area of .9999 is obtained which differs from the ideal condition by less than .001%. Thus, the amplifier response will accurately follow the ideal case under the conditions the dosimeter will most likely face during measurements.

Control/Readout Module

The second major component of the dosimeter is the Control/Readout module. This assembly is connected to the Diode Probe/Amplifier module via a 20 foot multiconductor cable.

The Control/Readout module contains the data acquisition circuitry needed to process the signals produced by the diode detectors. This module consists of 25 absolute value circuits (AVC), 25 voltage-to-frequency converters (VFC), 27 four decade counters, a voltage comparator, a clock up/down count section, and the circuitry necessary to interface the counters with the thermal printer used as the final readout device. Input to this module is via a 37 pin socket that accepts the multiconductor cable carrying signals from the diode amplifiers. A 30 conductor ribbon cable is attached to this socket allowing transfer of signals to a specific AVC, VFC, and decade counter group.

All of the circuitry associated with the Control/Readout module is located in a portable enclosure. Five Vector plugboards with 44 pin edge connectors are used to hold the integrated circuits and other discrete

components in the data analysis system. Four of these boards are identical and each contains six AVC, VFC, and decade counter sections as seen in Figure 29. The fifth board, seen in Figure 30, holds only one AVC, VFC, and counter section but houses the circuitry necessary to interface the data acquisition components with the thermal printer. Wire-wrap techniques are used to interconnect all of the circuit components.

Unless otherwise noted, CMOS integrated devices are used in the dosimeter since they exhibit low power dissipation levels, good noise immunity, multiple levels of voltage operation, and high speed.

Two power supplies, one providing $+5$ V, ±12 V and the other ±15 V, are available to supply the power needed by the dosimeter.

The Absolute Value Circuit

The addition of an absolute value circuit (AVC) in the dosimeter circuitry was necessary because negative voltages could be produced by the diode current amplifying electronics. Normally, the photovoltage applied to the VFC is positive; however, a positive dark current from each diode or a positive op amp input offset voltage could produce a negative voltage input to the VFC. This cannot be allowed so an AVC is included in each of the 25 data analysis sections to ensure always positive voltage input to the VFC.

The operation of the AVC can be understood by referring to Figure 31 (Gr78). Each circuit is located between a corresponding diode detector op amp and a VFC. The circuit uses a bipolar op amp (LM 1458) and an n-p-n (2N3904) transistor as its active components. In addition to producing a positive voltage output for either polarity input, a sign bit is available at the collector of the transistor. A positive input voltage to the op amp produces a high sign bit while a negative voltage produces a low bit value.

PACKAGE	DESIGNATION	DESCRIPTION
E	CD 4077	QUAD EXCL. NOR GATE
F	ICM 7217IJI	4 DECADE UP/DOWN CTR.
I	CD 4066	QUAD BILATERAL SWITCH
N	TRIM POTS	100,1k,10k OHMS
O	24 PIN SOCKET	VFC RANGE SWITCH
Q	VFC ASSOC. CKT.	VFC FREQUENCY SET
R	AD 537JD	VOLTAGE-TO-FREQUENCY CONVERTER
S	AVC ASSOC. CKT.	SIGNAL POLARITY
T	LM 1458	DUAL OP AMP

LEGEND
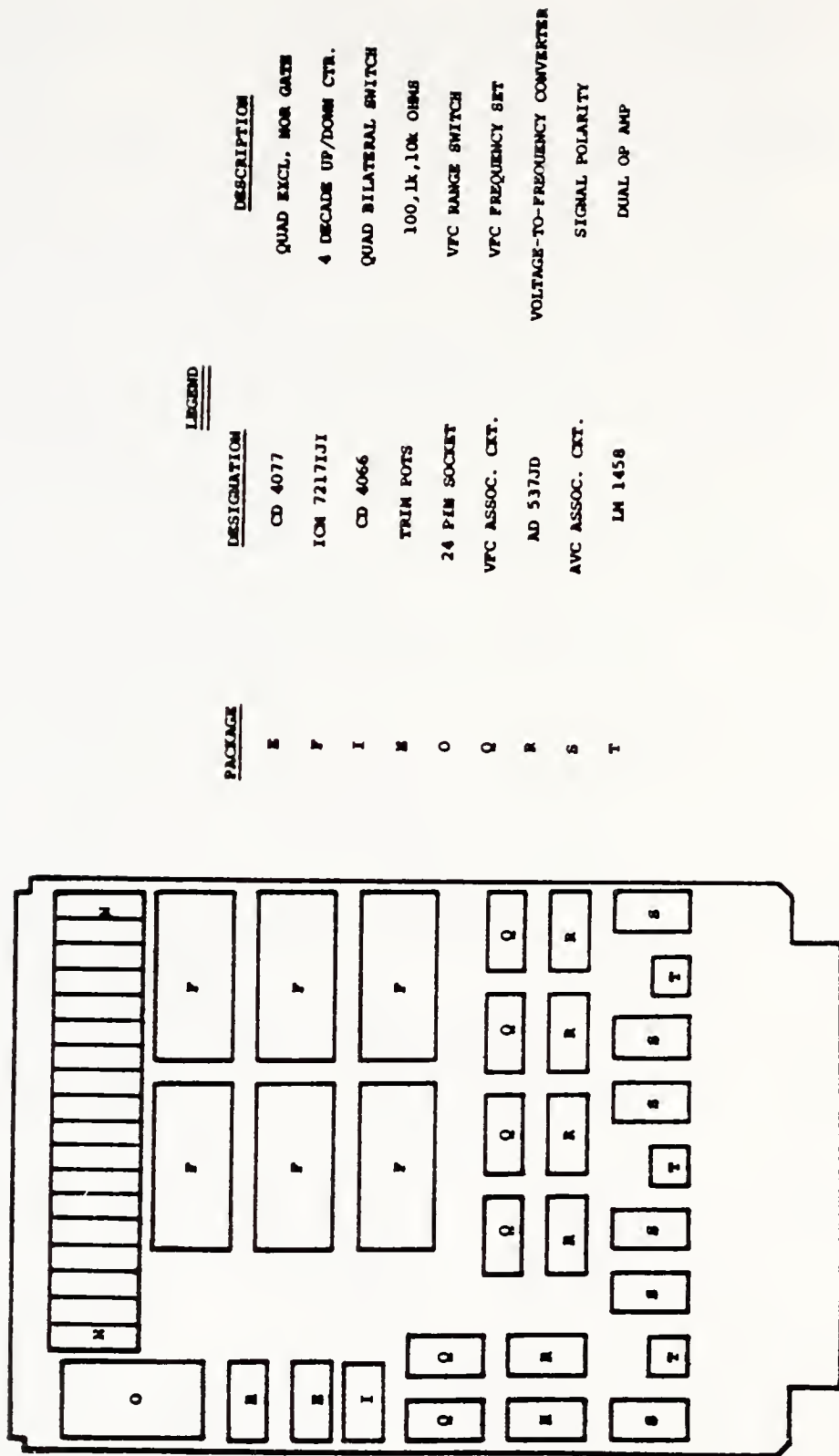
FIGURE 29. PACKAGE LAYOUT BOARDS 1-4

FIGURE 30. PACKAGE LAYOUT BOARD 5

LEGEND
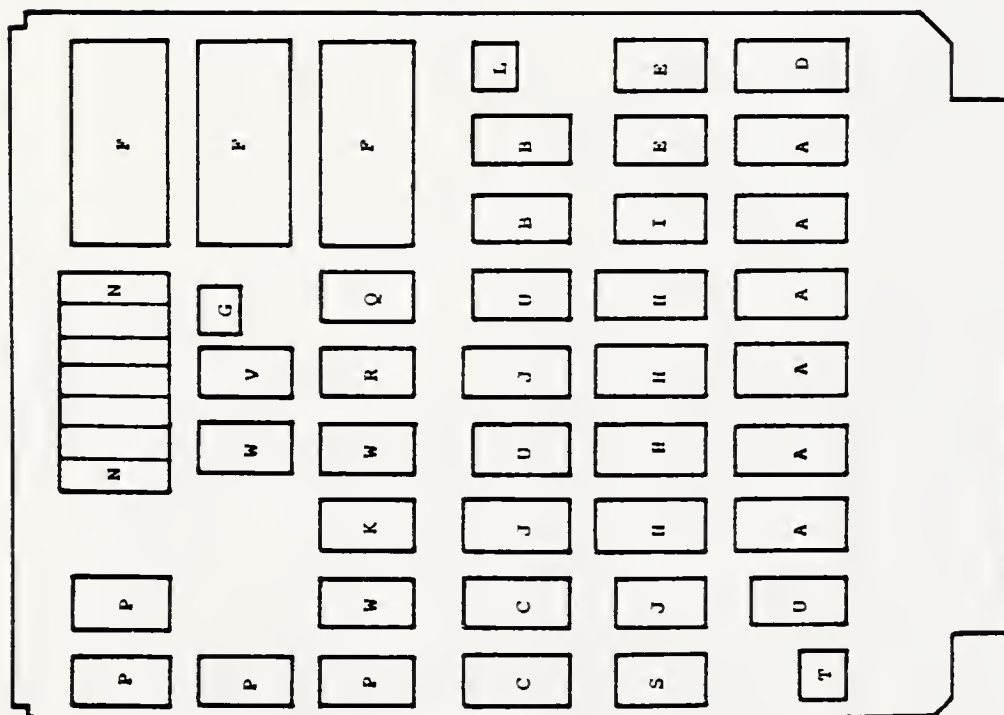
PACKAGE	DESIGNATION	DESCRIPTION
A	CD 4049	HEX INVERTER
B	CD 4071	QUAD OR GATE
C	CD 4043	QUAD R-S LATCH
D	CD 4050	HEX BUFFER
G	NE 555	TIMER OSCILLATOR
H	CD 4017	DECADE COUNTER/DIVIDER
J	CD 4098	MONOSTABLE MULTIVIBRATOR
K	LM 339	QUAD COMPARATOR
L	CD 40107	NAND BUFFER/DRIVER
P	14 PIN SOCKET	---
U	4098 ASSOC. CKT.	DELAY CIRCUITRY
V	555 ASSOC. CKT.	TIMER FREQUENCY
W	339 ASSOC. CKT.	HYSTERESIS CIRCUITRY

71

FIGURE 31. ABSOLUTE VALUE CIRCUIT (Gr78)

During operation of the dosimeter when a positive photovoltage is produced by the AD 515LH, the LM 1458 is disconnected from the circuit because a negative output turns off D_2 and the voltage is transferred directly to the VFC via resistors R_1 and R_2. If a negative voltage is developed by the AD 515LH, the output of the LM 1458 becomes positive turning on D_2 through zener diode D_1. Diode D_1 is included to ensure proper operation of the polarity bit transistor. Transistor Q_1 is turned on when the output of the LM 1458 is positive, thereby indicating a low output at the collector.

Because the input resistance is unequal for positive and negative voltage signals, a reversal voltage error of significant magnitude could be observed if the AD 515LH source resistance is greater that 10Ω or is not constant. This problem, however, is not faced because the $2k\Omega$ resistor located at the output of the AD 515LH is several magnitudes larger in resistance than the op amp output resistance over the voltage range of interest. This $2k\Omega$ resistance is simply subtracted from the value that R_1 would normally show if unity amplification is desired. The value of R_1 then becomes approximately $8k\Omega$. Individual matching of input resistance is required for each amplifier circuit.

The Voltage-to-Frequency Converter

A VFC is used to transform the analog signal from each diode amplifier into a digital form that can be processed and provide an equivalent exposure reading. A VFC and counter combination is used in the dosimeter to perform signal integration because of the expense and stability problems that were encountered when an amplifier and capacitor analog integrating design was first contemplated. A VFC possesses an inherently digital readout and integrating this digital signal produces a count total that is equivalent to the area under the voltage curve generated by the diode amplifiers (Te73).

The VFC used in the dosimeter is an Analog Device AD 537JD. This monolithic bipolar device consists of an input amplifier (buffer), a precision oscillator system (current-to-frequency converter), an internal reference generator, and a high current output stage (driver) (An78b). Figure 32 shows the circuit configuration of the AD 537JD used in the dosimeter. A full-scale input of 10 volts is determined by R_{scale}. The full-scale frequency is set by external components R_{scale} and C_1 (.001 uf polystyrene capacitor) and can be calculated from the relationship:

$F = V_{max}/10 \ C_1 \ R_{scale}.$

Figure 32 shows that R_{scale} has three ranges that are determined by three fixed (R_f) and three variable (R_v) resistors. These three ranges are utilized to set the frequency output for a specified input voltage and can be switched into the circuit using a three position, 25 pole rotary switch located on the Control/Readout module front panel. The three exposure ranges of 0-1, 10, and 100 R are defined by the proper resistance combination as indicated in Table 2.

Because of the input voltage characteristics of the VFC used in the dosimeter, two overscale ranges have been incorporated into the device as shown in Figure 33. Since the 0-1 R range is defined only to 1500 mV, an LED located on the front panel is turned on when an LM 339 comparator is tripped. The same LED is operated by another comparator that is activated when a 10 V level is exceeded on the 10 and 100 R ranges. Control of the particular comparator used for an exposure setting is determined by the front panel rotary switch.

The output of the VFC, taken from pin 14, had to be individually calibrated using R_v for each full-scale range. The resistor R_T was also individually selected to trim the input offset voltage of the input op

74

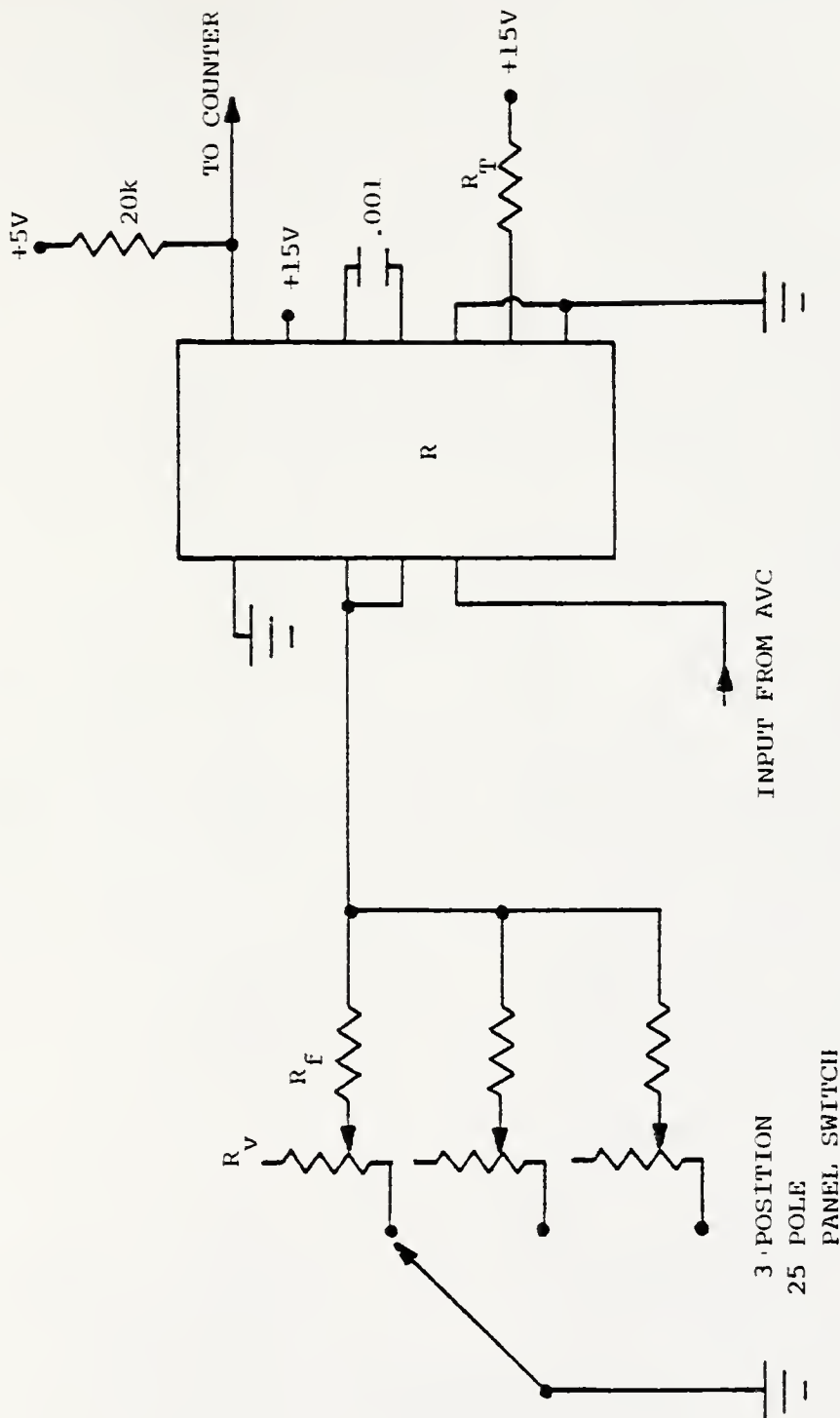FIGURE 32. VOLTAGE-TO-FREQUENCY CONVERTER CIRCUITRY

Table 2

Resistor Selection for Exposure Range

Full-scale Voltage (mV)	Full-Scale Frequency (Hz)	R_v (kΩ)	R_c (kΩ)	Exposure Range (R)
1,000	150,000	0.1	.91	0 – 1
10,000	100,000	1.0	9.1	0 – 10
10,000	10,000	10.0	91.0	0 – 100
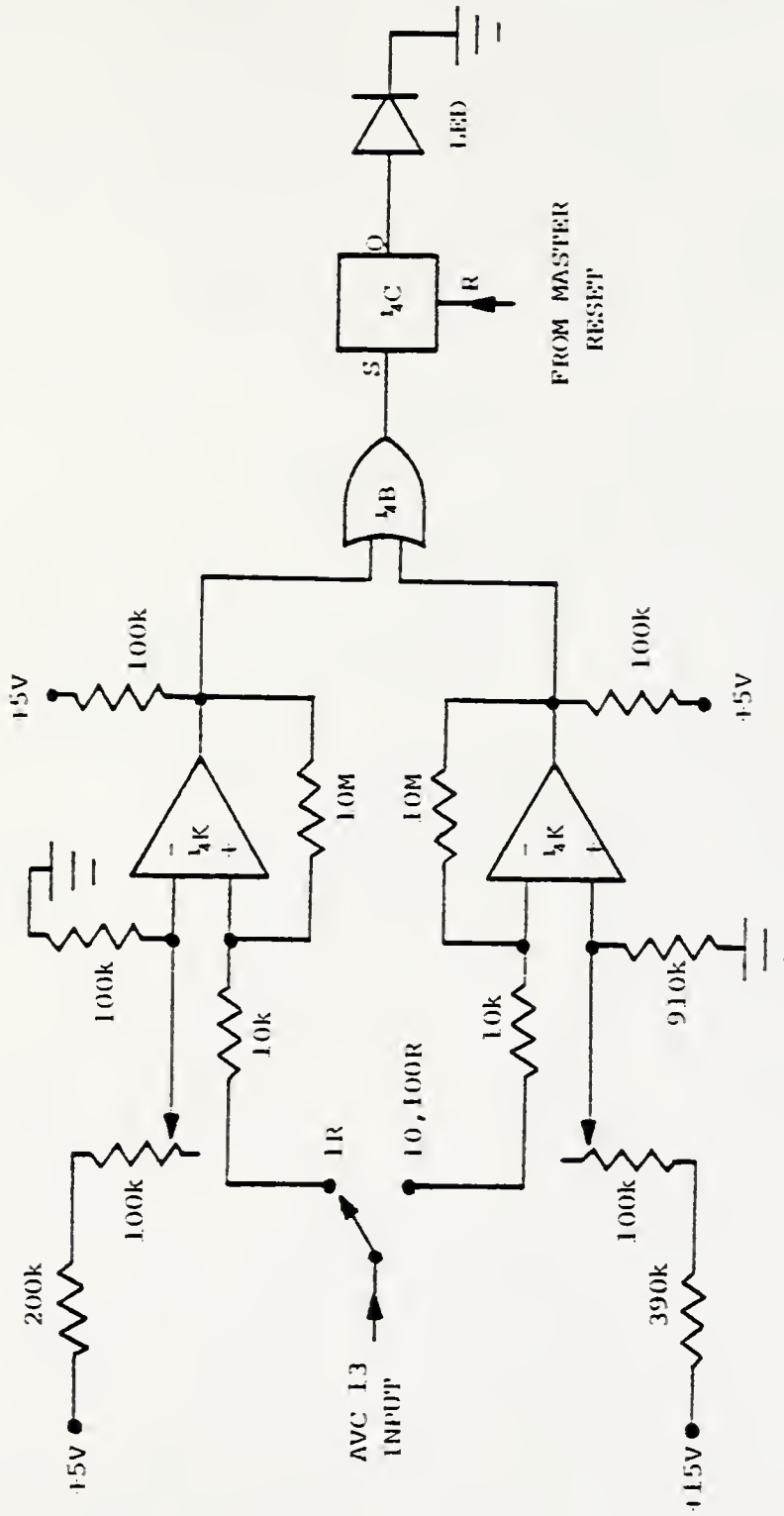
FIGURE 33. EXPOSURE RANGE OVERSCALE CIRCUITRY

amp for optimum frequency calibration in all ranges. The final output signal is a square wave of 5 V magnitude with a frequency proportional to the input voltage. Table 3 shows the variations in the output frequency over the input voltage averaged from all 25 VFC. From these results, it can be seen that there is a considerable overlapping of ranges. The correct integral exposure range and exposure rate range for a particular CT unit and exposure time will have to be experimentally determined at the time of measurement. This question is more fully analyzed in Chapter 4, SYSTEM OPERATION, CALIBRATION, AND EXPERIMENTAL RESULTS.

The Decade Counters and Associated Circuitry

The decade counters that are used to integrate the digital signals from the VFC are the central controlling components in the dosimeter. Each counter and its associated circuitry is responsible for data acquisition, storage, and display. Figure 34 shows a block diagram of the subsystems comprising the decade counter and associated control and readout circuitry. The dosimeter uses a Datel (Canton, Mass.) DPP-7A1 thermal printer for automatic sequential data printout and permanent exposure value storage.

The operation of the dosimeter is controlled by diode 13 (the center diode in the detector array) in that when the voltage from amplifier 13 exceeds a preset level (depending on dark current and offset voltage considerations), a voltage comparator turns on allowing the decade counter to accumulate pulses. The comparator also switches on the count up/down clock that is used to indicate scan time length and to control background subtract following completion of the scan.

The counters used in the dosimeter are Intersil (Cupertino, Calif.) ICM 7217IJI CMOS up/down four decade units (In78). A pin connection

Table 3

Variations in VFC Output Frequency

Range (R)	Volt Input (mV)	Calculated Frequency (Hz)	Average Actual Frequency (Hz)	% Freq. Variation
1	20	2,000	2,083	+ 4.0
	50	5,000	5,000	0.0
	500	50,000	48,570	- 2.9
	1,500	150,000	145,500	- 3.1
10	2	20	20.51	+ 2.5
	20	200	200	0.0
	50	500	500	0.0
	500	5,000	5,010	+ 0.2
	10,000	10,000	9,850	- 1.5
100	200	200	193.3	- 3.5
	500	500	500	0.0
	1,000	1,000	1,006	+ 0.6
	10,000	10,000	10,170	+ 1.7
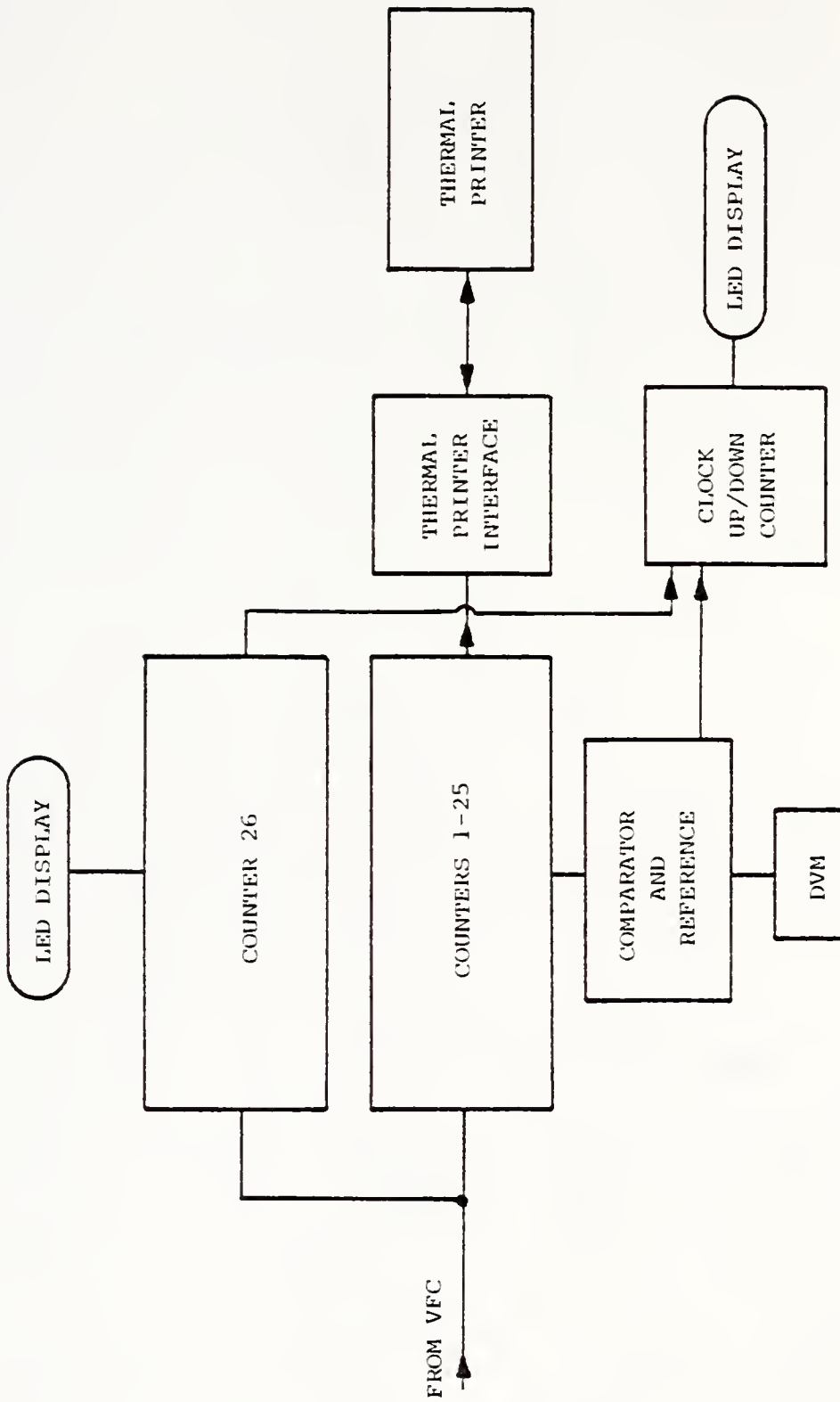
FIGURE 34. DECADE COUNTER AND ASSOCIATED CIRCUITRY

diagram for the counter can be seen in Figure 35. The counter provides
multiplexed 7-segment common anode outputs that can directly drive LED's
or the printhead of the thermal printer used as the output storage device.
The internal multiplexing (Mux) oscillator can be overridden by signals
produced in the thermal printer, thereby controlling digit display se-
quencing. Display blanking and unblanking is accomplished using digital
logic circuitry in coordination with control signals from the printer.

Twenty-five counters are used to integrate signals from the VFC
specific to each for readout by the printer. Counter 26 is connected in
parallel with counter 13 and is used to monitor the output of diode 13.
A National Semiconductors (Santa Clara, Calif.) NSB 7882 four decade
multiplexed LED display is found on the front panel of this module to ex-
hibit the integrated output of counter 26. This is provided to allow a
"real time" display of the scan data at the center diode (13) so that
exposure rate and data overrange information is immediately attainable.

A pin-by-pin description of the operation of the counters in associ-
ation with the control circuitry will now be presented.

The decade counter-pin 8. Pin 8 is used to input the square waves
from the VFC specific to each counter. The count input pin is provided
with a Schmitt trigger to allow operation in noisy environments and to
prevent multiple triggering.

The decade counter-pins 2, 9, 10, 14. The use of these pins is con-
trolled by the comparator, the absolute value circuitry, and the count
up/down clock. A diagram of the operation of these pins can be seen in
Figure 36.

Figure 37 shows the comparator circuitry that is used to sense the
switching point which turns on the clock counter (27) and the integrating
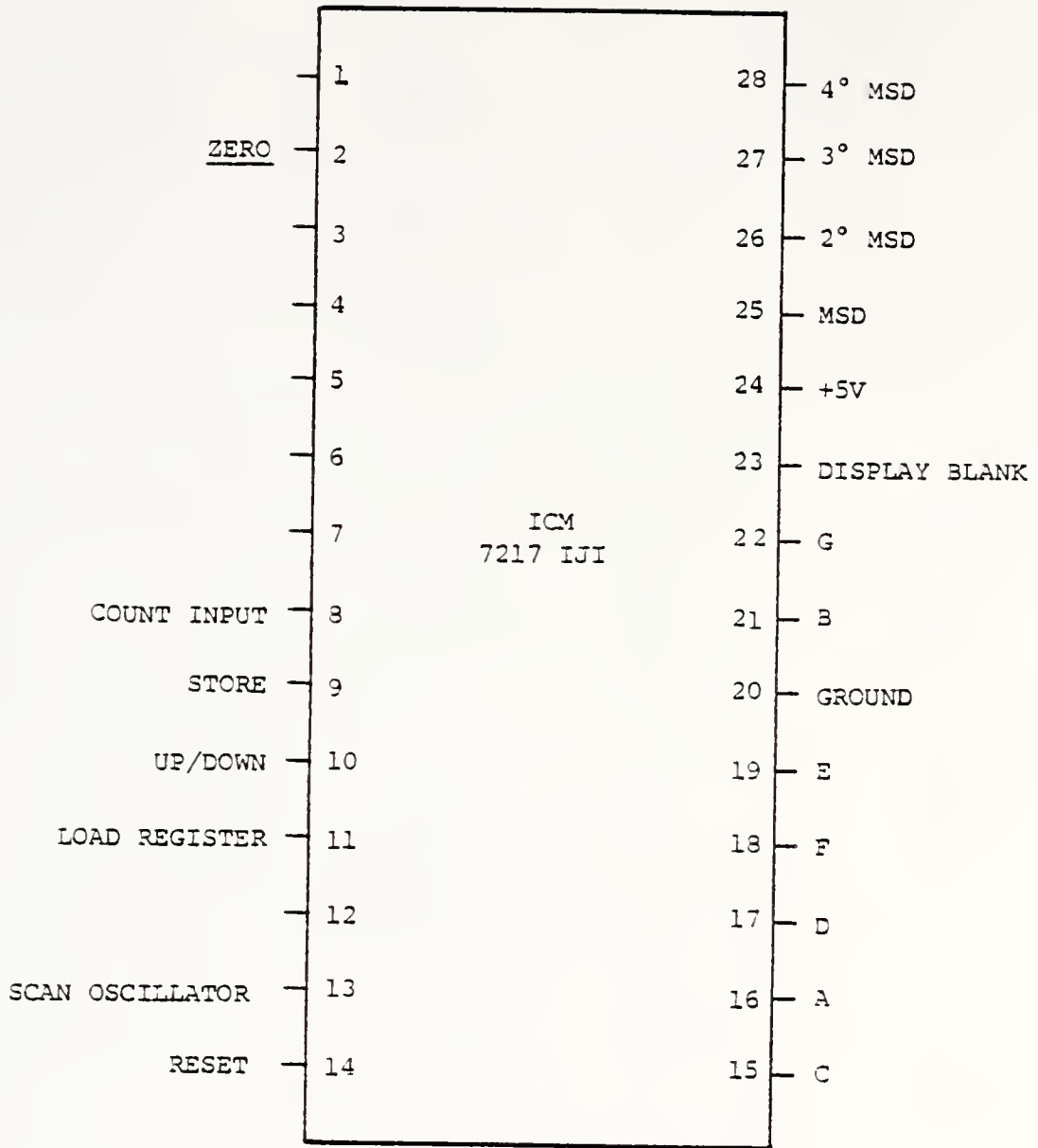
FIGURE 35.   PIN CONNECTION FOR ICM 7217 IJI

FIGURE 36. CIRCUITRY FOR COUNTER PINS 2,9,10,14
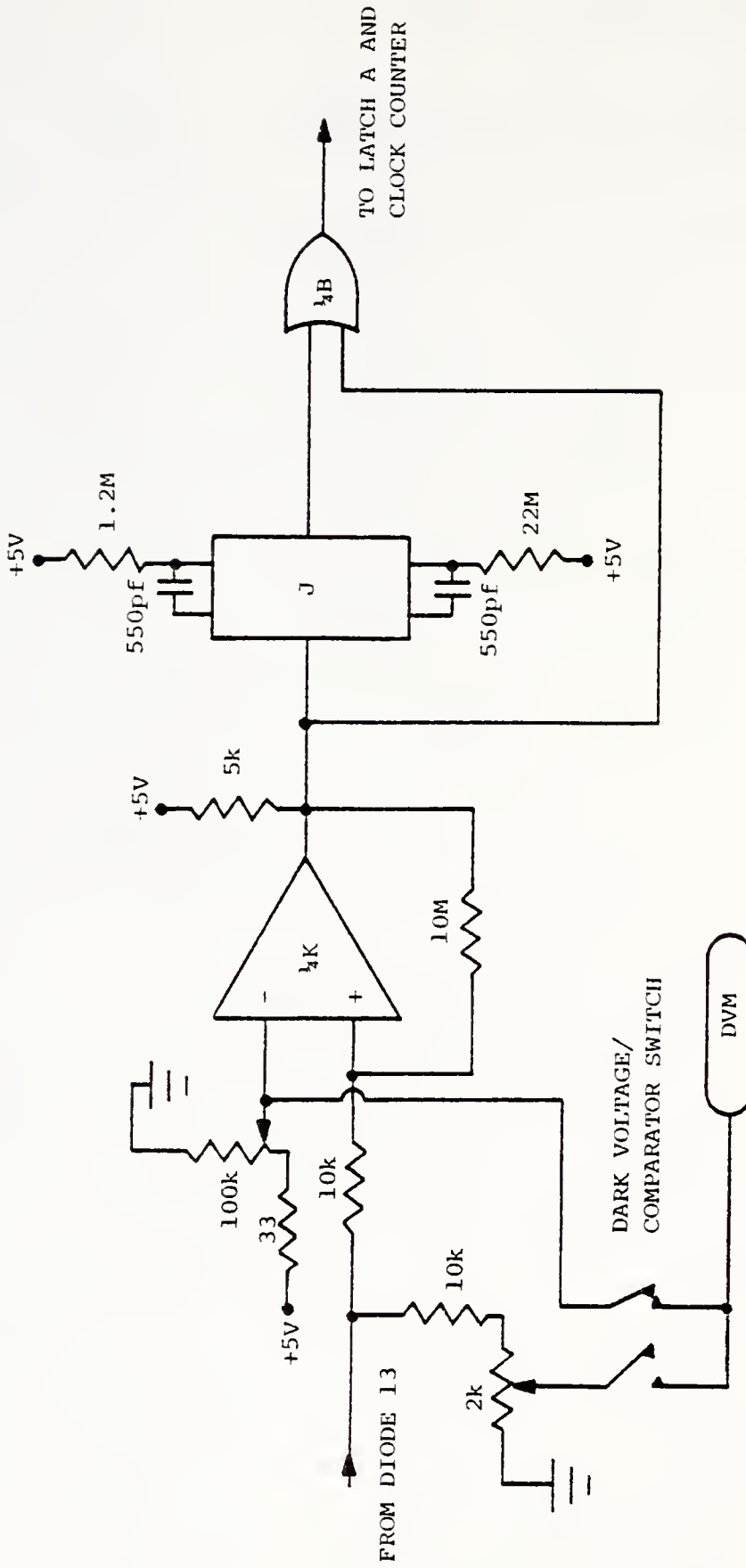
FIGURE 37. COMPARATOR TRIP CIRCUITRY

counters (1-26). The comparator uses hysteresis to assure proper switching in a potentially noisy circuit. Positive feedback is utilized to set up a finite input voltage difference between the on and off states of the comparator. A Datel DM-4100L digital voltmeter measures in mV, either the voltage from diode amplifier 13 (the CT scanner may be on or off), or the reference voltage, V_{ref}, that is used to set the trip point of the comparator depending on the position of switch S_1 (located on the front panel of the Control/Readout module). The reference voltage is taken from an output of the DVM and can be varied by a potentiometer located on the front panel. When the comparator is on, a ±5 V signal level is produced for control purposes.

Because pulsed beam CT scanners do not produce a continuous photon flux, a 4098 dual monostable multivibrator delay circuit has been incorporated into the circuit to ensure that the comparator stays at a high level between x-ray tube pulses. An OR gate enables the circuit to function in a continuous source beam as well as in the pulsed mode.

In Figure 38, the circuitry for the up/down clock counter logic is illustrated. An NE 555 oscillator used as an astable multivibrator producing a continuous 10 Hz square wave operates as the system clock. The clock pulses are directed into pin 8 of counter 27. The 7-segment counter output is displayed on a four decade LED display (NSB 7882) and indicates the length of time of the CT scan. The LED display can measure a scan time up to 999.9 seconds.

Figure 36 shows the circuitry configured around counter input pins 2, 9, 10 and 14 for counters 1-27. Pin 2 on counter 27 and pin 9 on counters 1-26 operate in conjunction in order to store data in the output latches of each 7217 for later retrieval. When the comparator is tripped

FIGURE 38. CLOCK UP/DOWN COUNTER CIRCUITRY

at the beginning of a scan, latches B and C use the comparator signal an

the high level from the Zero (pin 2) output from counter 27 to allow con-

stant updating of the output latch in counters 1-26. Pin 2 produces a

low level when the counter content is at zero. When the scan is com-

pleted, and automatic background subtract is performed after which the

counter output latches are set (i.e., data stored) in readiness for read-

out. Resetting of each counter is performed through Latch A using a man-

ual switch located in the front panel. The reset switch is operated

through a 4043 latch to make it bounceless. Counter 26 requires direct

data output into a four decade LED so the addition of a 4077 and a 4049

to its pin 9 store input allows the display to be erased (by the manual

reset) before another scan is started. Pin 10 sets the up or down count

mode. When a high polarity AVC sign bit is present and the comparator

is on (corresponding to a positive photocurrent), the up count mode is

chosen. The comparator goes low when the CT scan is completed. If the

voltage from diode amplifier 13 is now negative (indicating a positive

dark current or offset voltage), the background subtract control will

cause counters 1-26 to count up, thereby compensating for the constant

negative signal error. The reverse occurs if the quiescent diode ampli-

fier voltage is positive. The output of Latch C is connected through a

4049 to an LED indicator located on the front panel that actuates when

the background subtract function is completed.

The decade counter-pins 11, 13. Pins 11 and 13 of counters 1-25

are used along with some associated circuitry as the control interface

between the data analysis system previously described and the thermal

printer. Figure 39 is a diagram of the counter/thermal printer inter-

face components. Pin 13 allows outside overriding of the onboard Mux
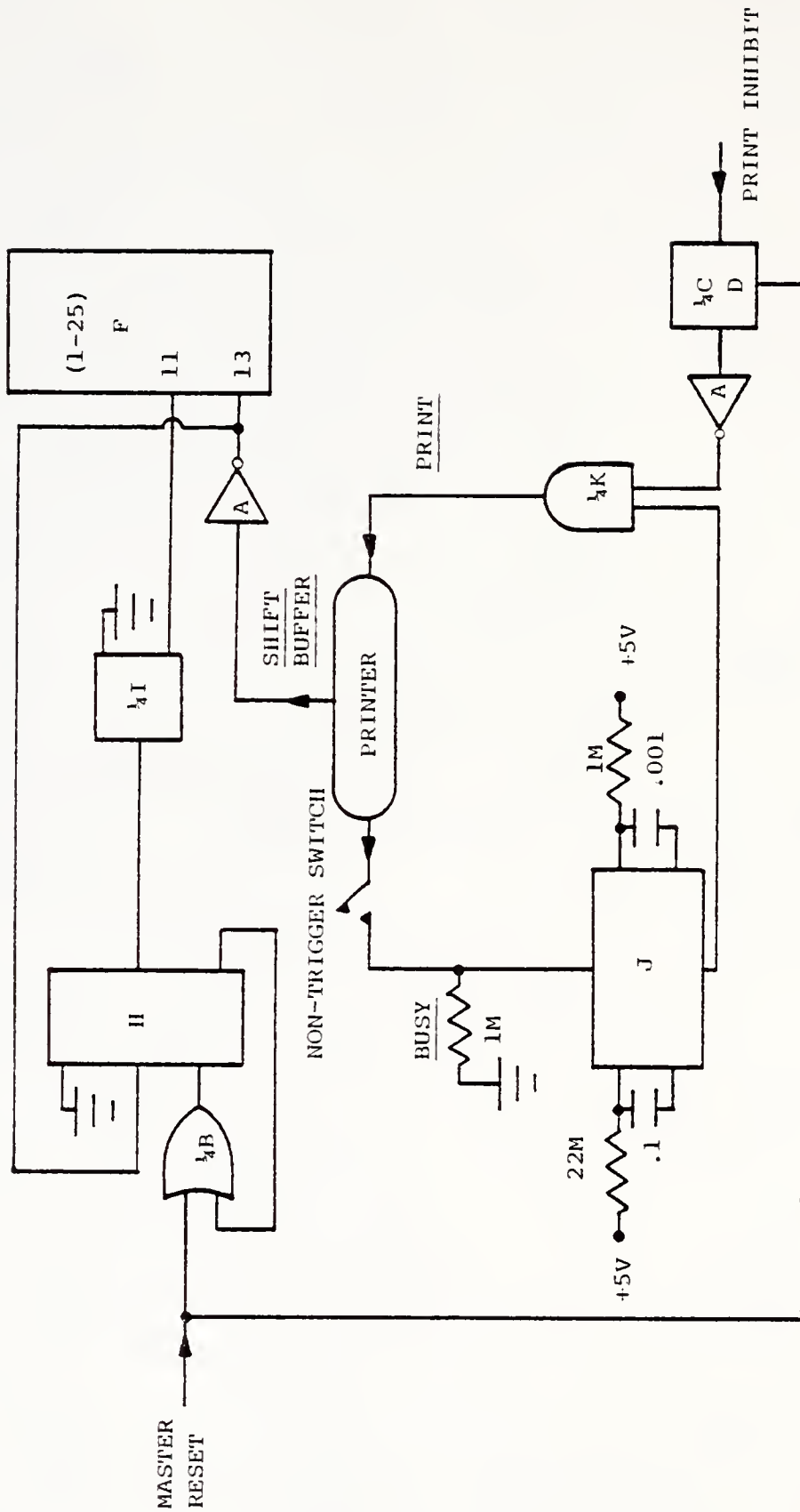
FIGURE 39.   COUNTER LOAD REGISTER AND PRINTER HANDSHAKE CIRCUITRY

scan oscillator of each counter. The thermal printer used in the do-
simeter produces a number of internal signals that are used to provide
controls for the operation of the data analysis circuitry. A Shift
Buffer signal taken from the printer is inverted and used to trigger the
Mux sequencing input (pin 13) that selects what decade digit is to be
accessed next. The Shift Buffer signal is high for 2 msec and low for
25 msec. This provides adequate time for data readout from a particular
digit which occurs during the low state between Shift Buffer pulses.
Figure 40 shows the timing chart for this operation. The entire sequence
of print startup is controlled by a manual Print signal caused by the
actuation of a switch located on the thermal printer front panel. The
operation of this print switch begins the automatic printout of exposure
data from each counter. The Print pulse is generated during each succeed-
ing print cycle using a "handshake" arrangement with a Busy signal from
the printer that remains high during printout and paper advance activi-
ties. A delay circuit using a 4098 dual monostable multivibrator facili-
tates this operation. At the end of the first cycle, the Busy signal
goes low causing a pulse delayed by about 220 msec to be sent to the re-
mote Print control in the printer, thus allowing automatic sequencing to
counter 2 and subsequent printout of the remaining counters. When the
twenty-fifth cycle has been completed, an inhibit signal from the display
multiplexing system (to be discussed) prevents further Print signals
reaching the printer unless the manual print switch first is engaged. A
switch is present in the Busy line to prevent premature operation of the
printout circuitry.

The main feature of the ICM 7217 that ensured its choice as the
counter for the system is that provided by pin 11--the load register (LR)
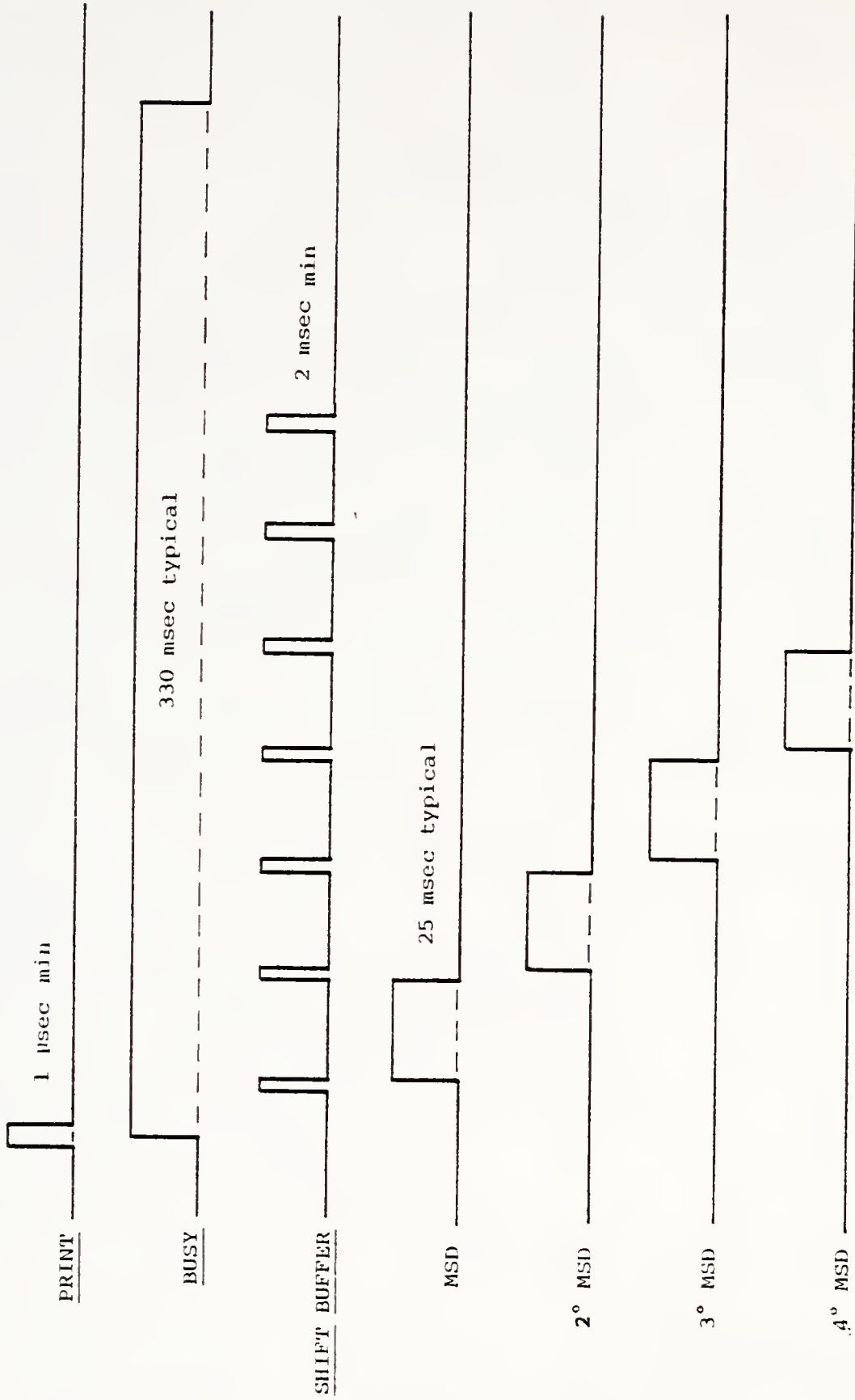
FIGURE 40. TIMING CHART FOR MUX SCAN OSCILLATOR OVERRIDE AND
LOAD REGISTER FUNCTION FOR ONE PRINT CYCLE

control. When the LR input is forced to ground, the 7-segment display driver outputs (pins 15-19, 21, 22) are disabled, the Mux oscillator is inhibited (including any overriding signals), and the internal digit select Mux counter is reset to the most significant digit (MSD). This is a crucial control because the thermal printer begins printing from left to right (i.e., starting with the MSD). Therefore, when the printer begins the print cycle, the data value for the first character printed (the MSD) must be present at the printhead input. This synchronizing operation is accomplished using a 4017 decade decoder, a 4066 bilateral switch, and the Shift Buffer input signals.

After initial system reset, activation of the manual print switch causes the Shift Buffer signal to be sent by the printer. At this point pin 3 of the 4017 is high inhibiting the Mux oscillator through the 4066. When the first pulse from the shift buffer inputs into the 4017, pin 3 goes low, turning off the 4066 (releasing the LR pin) and allowing sequencing through the digit select counter starting with the MSD. The output drivers of the particular digit chosen are only active when the Shift Buffer pulse is low. The second MSD is selected by the second Shift Buffer signal. The sequencing continues until the fifth Shift Buffer pulse is inputted into the 4017. Although the printer has the capability of displaying six digits, the last two digits have been externally blanked since the counter output covers only four decades. Pulses 5 and 6 from the Shift Buffer perform no function. Pulse 7 resets the 4017 to zero and holds the LR input of all counters low, thereby resetting the Mux counter to the MSD position. This sequence reoccurs during each cycle to ensure proper print coordination between the counters and the thermal printer.

The decade counter-pins 23, 15-19, 21, 22. The control that enables
the 7-segment output from each counter to be transferred to the printer
is pin 23--display blanking. Figure 41 shows the circuitry of the Mux
system enabling or disabling the blanking control of all 25 counters.
Normally, all outputs of the three 4017's are low. A 4049 is provided
to invert this level causing blanking of all counter 7-segment outputs.
During the initiation of the print cycle by the manual switch, the printer
Busy output goes high clocking a pulse the length of the print cycle into
the 4017 decoder. This signal turns on the first channel output which
after passing through the 4049, unblanks the display drivers in readiness
for printout in conjunction with the Shift Buffer (LR control) signals
previously described. After completion of the first print cycle, the
Busy signal goes low initiating a 4098 delayed pulse (see Figure 38) to
go high 220 msec later for 1 msec providing a Print command that now
automatically reoccurs during each of the remaining 24 print cycles. At
the completion of the 25 print cycles, a 4098 delay resets all 4017 coun-
ters allowing another printout of all decade counters should that option
be desired. Print inhibition is obtained after all counters are examined
(see Figure 39) using a 4043 and a 4077 to prevent the delayed Print
pulse from reaching the printer after the Busy signal goes low at the end
of the twenty-fifth cycle.

Because of the blanking control available on the 7217, like 7-segment
outputs (segments a-g) from each counter can be tied together so that only
7 lines containing the segment information are directed into the printer.
Each line feeds into a 7405 hex inverter which, in turn, drives a tran-
sistor triggering the corresponding segment in the printhead.
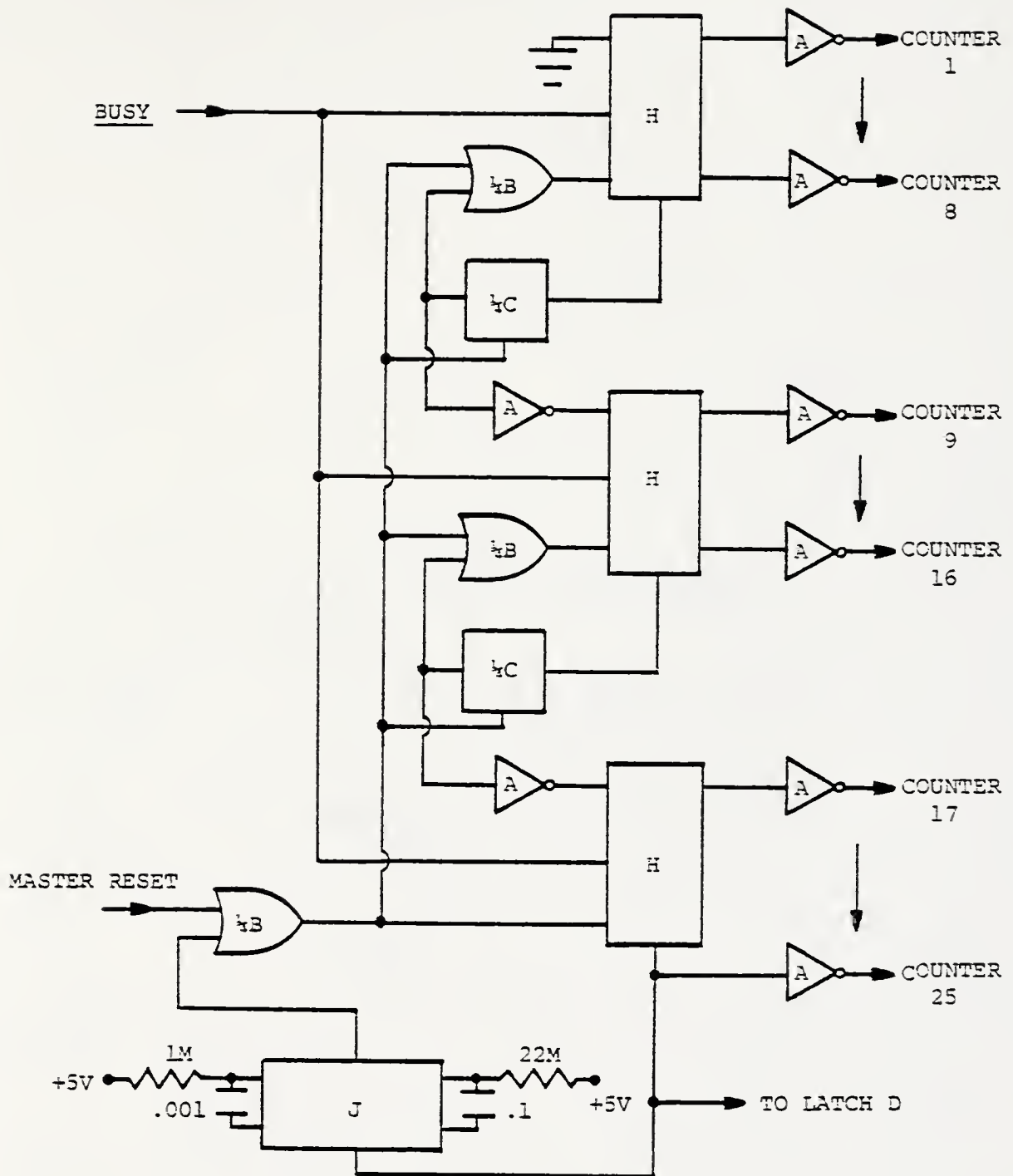
FIGURE 41. DISPLAY BLANKING CONTROL CIRCUIT

The decade counter-pins 25-28. Pins 25-28 are the digit select out-
puts that are used only on counters 26 and 27 so that the LED Mux display
may be directly driven.

The decade counter-pins 24, 20. Pin 24 is used to input the +5 V
power required by the counter. The system ground is connected to pin
20.

Power supplies

The power requirements for the components used in the dosimeter are
listed in Table 4. A Motorola PLT 810 triple output power supply pro-
vides ±5 V at a maximum output current of 4 amps. The +5 V capability is
used primarily by the digital logic circuitry. A ±12 V output from the
PLT 810 at 0.7 amps maximum is used by the 25 AD 515LH op amps in the
Diode Probe/Amplifier module and is transferred to that unit by the multi-
conductor cable. A Datel BPM-15/200 ±15V supply provides up to 200 mA
of current for use by the AVC op amps and the VFC. Both of these power
supplies are highly regulated to produce low ripple power to the dosimeter
electronics.

Bypassing on all wire-wrap boards between ±12 V, ±15 V, and +5 V
lines and ground is provided using 22 uf tantalum and .01 uf ceramic
capacitors. Electromagnetic shielding is provided around the power sup-
plies and power wires to eliminate any 60 Hz signals that could influence
circuit operation.

Table 4

Power Supply Requirements for the Dosimeter

Component	# Needed	Total Current Required (ma)			
		+5V	12V	15V	
AD 515LH	25	--	37.5	--	
H11F3	25	150	--	--	
LM 339	1	5	--	--	
DM 4100L	1	400	--	--	
NSB 7882	2	600	--	--	
LM 1458	13	--	--	65	
AD 537JD	25	--	--	37.5	
ICM 7217	27	25	--	--	
NE 555	1	5	--	--	
Misc. CMOS	--	100	--	--	
		1260	37.5	102.5	

CHAPTER IV
SYSTEM OPERATION, CALIBRATION, AND EXPERIMENTAL RESULTS

The following discussion provides a description of the system
operation, and includes preliminary information on the device calibra-
tion obtained from initial experimental testing. Further investiga-
tions into the response of the dosimeter will be performed to meet the
final specified operational requirements.

System Operation

The actual operation of the CT dosimeter is straightforward but
requires a complete understanding of its capabilities and limitations.
A working knowledge of the magnitude and mode of delivery of the radia-
tion flux it will be required to measure should be available to the
operator.

Basically, after connecting the Diode Probe/Amplifier and Control/
Readout modules together via the multiconductor cable, power may be
applied to the system. At this point, the thermal printer non-retrigger
front panel switch should be in the off position. The reset switch
should be depressed to initialize the system. The dark voltage compara-
tor (DVC) switch should be set to the dark voltage read position so a
measurement of the voltage from diode 13 can be made. Upon completion
of this reading, the DVC switch should be placed into the comparator set
position and a trip selected using the potentiometer provided on the
front panel at a point about 10 mV greater than the dark voltage reading

previously obtained. The voltage readings are made using the panel DVM.
The DVC switch may then be set back into the dark voltage read position
so that a relative reading of the diode photovoltage can be made during
the irradiation.

The expected exposure range is next chosen using the 3 position
rotary switch. The position of the High/Low scan rate switch will have
to be experimentally determined for a particular set of irradiation
conditions. Most likely the High position should be used to make the
first set of measurements in an exposure range. If the comparator is
not being tripped, the low range may then be used to make a series of
test measurements. Several readings should be made for each experimental
condition to be tested. After the completion of an irradiation, the
non-retrigger switch is placed in the on position and the print switch
is depressed on the thermal printer to dump the exposure data.

Calibration and Results

A limited amount of experimental data has been gathered from the
dosimeter. These early results have been obtained using the Siemens
Orthovoltage single-phase x-ray device located at the Shands Teaching
Hospital, Gainesville, Florida, as the radiation source.

The first series of tests was designed to indicate the reproduci-
bility of the data obtained from the twenty-five diodes. Table 5 shows
the average counts/second and percent variation between a series of
four irradiations of the diode probe performed with the probe placed
into a 6.5 cm thick plexiglass phantom. Reproducibility between runs
varies between 1 and 12% and averages about 4%. The results show a
large amount of variation between the radiation response of the diodes

Table 5

Reproducibility Studies of the Diode Probe

Diode	Ave. Count/s	% Variation		Diode	Ave. Count/s	% Variation
1	252	4		14	138	8
2	--	--		15	96	2
3	364	1		16	161	3
4	599	1		17	--	--
5	706	1		18	12	12
6	760	1		19	54	3
7	103	6		20	143	3
8	707	1		21	643	6
9	318	5		22	88	4
10	206	3		23	14	7
11	832	6		24	172	4
12	626	2		25	--	--
13	287	6				

(120 kVp, 4 mA, 60 cm SDD, 4 mm aluminum Total Filtration)

necessitating calibration factors for each detector. This variation may
be due largely to the presence of air in the probe since in these early
runs the diodes were not surrounded by a potting compound. For some
diode positions no data can be given because of problems still to be in-
vestigated.

Table 6 shows the results of irradiating the diode probe at energies
of 100 and 120 kVp, respectively. A calibration factor in mR/count has
been determined using a Victoreen R-meter and ionization chamber as the
exposure reference. The effect of increasing the beam energy is apparent
from these results.

A more detailed series of irradiation tests is contemplated to more
fully document the capabilities of the system.

Table 6

Calibration of Diode Probe at 100 and 120 kVp

Diode	100 kVp Ave. Count/sec	mR/count	120 kVp Ave. Count/sec	mR/count
1	719	.04	1,143	.04
2	--	--	--	--
3	--	--	--	--
4	1,074	.03	1,216	.04
5	715	.04	675	.07
6	777	.03	774	.06
7	156	.17	167	.28
8	556	.05	719	.06
9	204	.13	333	.14
10	188	.14	226	.20
11	449	.06	779	.06
12	--	--	613	.08
13	164	.16	236	.19
14	270	.10	476	.10
15	78	.35	95	.48
16	155	.17	129	.36
17	--	--	--	--
18	298	.09	273	.17
19	47	.57	54	.85
20	137	.20	144	.32
21	456	.06	625	.07
22	75	.36	85	.54
23	11	2.45	14	3.29
24	150	.18	163	.28
25	--	--	--	--

(4 MA, 80 cm SDD, 4 mm aluminum Total Filtration); 100 kVp → 27 mR/S, 120 kVp → 50 mR/s)

CHAPTER V
CONCLUSIONS AND RECOMMENDATIONS

As stated in the Introduction, the goal of this project was to produce an instrument that could expeditiously measure the radiation exposure a patient could receive during a CT scan. Such a device has been conceived, produced, and found to be operationally functional.

The main emphasis of this research has been to demonstrate the feasibility of silicon p-i-n diodes as radiation detectors. To this end, the diode probe and accompanying amplifying electronics have been developed and tested. The choice of output medium was left to the investigator and a satisfactory system was designed and constructed. Perhaps most importantly, the design of the diode module allows it to be interfaced with many different types of output devices especially microprocessors. It is hoped that future investigators will take up the challenge of incorporating this proven technology into as yet undeveloped systems.

BIBLIOGRAPHY

(Ag78)   Agee, O.F., 1978, personal communication.

(Al77)   "Alderson 'Catphan' Phantom," 1977, Alderson Research Labora-
           tories, Inc.

(Am63)   Ammerlaan, C.A.J. and Mulder, K., 1963, Nucl. Instrum. and
           Meth., 21, 97.

(An78a)   Analog Devices Data Acquisition Products Catalog, 1978, Analog
           Devices, Inc., 7.

(An78b)   Analog Devices Data Acquisition Products Catalog, 1978, Analog
           Devices, Inc., 475.

(As76)   Ashe, J.B., 1976, Radio/Nucl. Med. Mag., 6, 46.

(Ba64)   Baily, N.A. and Kramer, G., 1964, Radiation Res., 22, 53.

(Ba65)   Baily, N.A. and Hilbert, J.W., 1965, Physics Med. Biol., 10, 41.

(Ba76)   Barrett, H.H., Gordon, S.K., and Hershel, R.S., 1976, Computers
           Biol. Med., 6, 307.

(Ba77)   Bassano, D.A., Chamberlain, C.G., Mosley, J.M., and Kieffer, S.A.,
           1977, Radiology, 123, 455.

(Ba78)   Banta, H.D., 1978, in Proceedings of 9th Annual National Confer-
           ence on Radiation Control, 74.

(Bl62)   Blankenship, J.L., and Borkowski, C.J., 1962, I.R.E. Trans.
           Nucl. Sci., NS-9, 181.

(Br61)   Brown, W.L., 1961, I.R.E. Trans. Nucl. Sci., NS-8, 2.

(Br76)   Brooks, R.A., and DiChiro, G., 1976, Med. Phys., 3, 237.

(Bu77)   Budinger, T.F. and Gullberg, G.T., 1977, in Reconstruction
           Tomography in Diagnostic Radiology and Nuclear Medicine, 315.

(Bur77)   "The Bureau of Radiological Health - A Look at FDA's Program to
           Protect the American Consumer from Radiation," 1977, HEW/FDA
           77-8032.

(Ca77)   "Capintec Tomorad I Dosimetry System," 1977, Capintec, Inc.

(Ce69)   Cember, H., 1969, _Introduction to Health Physics._

(Ch77)   Chesler, P.A., Aronow, S., Correll, J.E., Ricderer, S. and Pelc,
           N., 1977, in _Reconstruction Tomography in Diagnostic Radiology
           and Nuclear Medicine_, 49.

(Cho77)   Cho, Z.H., Eriksson, L., and Chan, J., 1977, in _Reconstruction
           Tomography in Diagnostic Radiology and Nuclear Medicine_, 393.

(Cl76)   Cloe, L.E., 1976, _Am. J. Roentg._, _127_, 187.

(Co64)   Coleman, J.A., and Rodgers, J.W., 1964, _IEEE Trans. Nucl. Sci._,
           _NS-11_, 213.

(Co76)   "The Computer Tomography (CT or CAT) Scanner and Its Implica-
           tion for Health Policy," 1976, United States Congress, Office
           of Technology Assessment.

(Co77)   "Computer Program Being Developed for CT Dose-Image Evaluation,"
           1977, _BRH Bulletin XI._

(Com77)   _Computer Tomography Scanning - A Policy Statement_, 1977, Insti-
           tutes of Medicine, National Academy of Science.

(Co78)   "Cooperative Survey of CT System Image and Dose Initiated," 1978,
           BRH Bulletin XII.

(CT76)   "The CT 5005 General Diagnostic Scanner," 1976, EMI Medical, Inc.

(CT77)   "The CTR-100 Neurodiagnostic Scanner, 11," 1977, EMI Medical,
           Inc.

(CT78)   "CT/T Technology Continuum - Technical Performance of the CT/T
           System, 1978, General Electric Comp.

(De64)   Dearnaley, G., 1964, _Nucleonics_, _22_, 79.

(De77a)   Derenzo, S.E., 1977, _IEEE Trans. Nucl. Sci._, _NS-24_, 881.

(De77b)   Derenzo, S.E., Zaklad, H., and Budinger, T.F., 1977, in _Recon-
           struction Tomography in Diagnostic Radiology and Nuclear Medicine_,
           343.

(De78)   "The Development of a Dosimeter," 1978, BRH Negotiated Contract,
           #223-78-6002.

(Du69)   Durling, A.E., 1969, _Introduction to Electrical Engineering._

(El78)   _El Tec Instruments Product Catalog_, 1978, Eltec Instruments,
           Inc.

(Ev78)   Evens, R.G., 1978, in _Proceedings of 9th Annual National Confer-
           ence on Radiation Control_, 69.

(Fa78)   "Farmer Portable Dosemeter," 1978, Nuclear Enterprises, Inc.

(Fi77)   Fineberg, H.U., Bauman, R., and Sasman, M., 1977, J.A.M.A., 238, 224.

(Fo63)   Fowler, J.F., 1963, Phys. Med. Biol., 8, 1.

(Fo66)   Fowler, J.F., 1966, in Radiation Dosimetry II, 291.

(Ge77)   Genna, S., Pang, S.C., Burrows, B.A., 1977, in Reconstruction Tomography in Diagnostic Radiology and Nuclear Medicine, 139.

(Go77a)   Goodenough, D.J., Weaver, K.E. and Davis, D.O., 1976, Optical Eng., 16, 52.

(Go77b)   Goodenough, D.J., Weaver, K.E. and Davis, D.O., 1977, in Reconstruction Tomography in Diagnostic Radiology and Nuclear Medicine, 225.

(Gr71)   Graeme, J.G., Tobey, G.E., and Huelsman, L.P., 1971, Operational Amplifiers - Design and Applications.

(Gr78)   Grant, D., 1978, "Applications of the AD537 I.C. Voltage-to-Frequency Converter," Analog Devices, Inc.

(Gu62)   Guldbrandsen, T. and Madsen, C.B., 1962, Acta Radiol., 58, 226.

(Ho73)   Hounsfield, G.N., 1973, Brit. J. Radiol., 46, 1016.

(HT76)   "HT Tomography Phantom," 1976, Atomic Development Corp.

(In76)   Introduction to Computed Tomography, 1976, General Electric Company.

(In78)   "Intersil's ICM 7217 Series CMOS 4 Digit Up/Down Counter-Decoder-Driver-Preliminary Specifications," 1978, Intersil, Inc.

(Jo62)   Jones, A.R., 1962, I.R.E. Trans. Nucl. Sci., NS-9, 17.

(Jo63)   Jones, A.R., 1963, Phys. Med. Biol., 8, 451.

(Jo74)   Johns, H.E. and Cunningham, J.R., 1974, The Physics of Radiology.

(Ju77)   Jucius, R.A. and Kambic, G.X., 1977, in Proceedings of the Society of Photo-Optical Instrumentation Engineers, 127, 1.

(Ka77)   Kambic, G.X. and Wake, R.H., 1977, IEEE Trans. Nucl. Sci., NS-24, 874.

(Kl73)   Klevenhagen, S.C., 1973, Acta Radiol., 12, 124.

(Kl77a)   Klevenhagen, S.C., 1977, Phys. Med. Biol., 22, 353.

(Kl77b)   Klevenhagen, S.C., 1977, Phys. Med. Biol., 22, 368.

(Kl77c)   Klevenhagen, S.C., 1977, Phys. Med. Biol., 22, 777.

(Kl78)   Klevenhagen, S.C., 1978, Med. Phys., 5, 52.

(Le74)   Ledley, R.S., Wilson, J.B., Golab, T. and Rotolo, L.S., 1974, Computers Biol. Med., 4, 145.

(Le76)   Ledley, R.S., 1976, Computers Biol. Med., 6, 239.

(Li75)   Little, A.D. (Inc.), 1975, A Health Planning Document; Compuized Tomographic Scanning Systems.

(Lo58)   Loferski, J.J. and Rappaport, P., 1958, Phys. Tev. III, 432.

(Mc74)   McCullough, E.C., Baker, H.L., Houser, O.W., and Reese, D.F., 1974, Radiology III, 709.

(Mc75)   McCullough, E.C., 1975, Med. Phys., 2, 307.

(McD75)   McDavid, W.D., Waggener, R.G., Payne, W.H., Dennis, M.J., 1975, Med. Phys., 2, 321.

(Mc76)   McCullough, E.C., Payne, J.T., Baker, H.L., Hattery, R.R., Sheedy, P.F., Stephens, D.H., Gedgaudus, E., 1976, Radiology, 129, 173.

(Mc77)   McCullough, E.C. and Payne, J.T., 1977, Med. Phys., 4, 85.

(Mi72)   Millman, J. and Halkias, C., 1972, Integrated Electronics: Analog and Digital Circuits and Systems.

(Mo77)   Monahan, W.G., 1977, IEEE Trans. Nucl. Sci., NS-24, 567.

(Mor77)   Morgan, T., 1977, personal communication.

(Mo78)   Moore, M.M., Cacak, R.K. and Hendry, W.R., 1978, Abstract in 1978 AAPM Annual Meeting Program.

(Mot78)   Motz, J.W. and Danos, M., 1978, Med. Phys., 5, 8.

(Oh76a)   "Ohio Nuclear's Delta-Scan50--Total Body Computer Tomography Scanners," 1976, Ohio Nuclear, Inc.

(Oh76b)   "Ohio Nuclear's Delta-Scan25--Typical Dosages in Rads," 1976, Ohio Nuclear, Inc.

(Oh76c)   "Ohio Nuclear's Delta-Scan 2020," 1976, Ohio Nuclear, Inc.

(Pa76)   Payne, J.T. and McCullough, E.C., 1976, Appl. Radiol., 5, 53.

(Pe73)   Perry, B.J. and Bridges, C., 1973, Brit. J. Radiol., 46, 1048.

(Pet73)   Petushkov, A.A., and Parker, R.P., 1973, Phys. Med. Biol., 18, 235.

(Pe77)   Pentlow, K.S., Beattie, J.W. and Laughlin, J.S., 1977, in
           Reconstruction Tomography in Diagnostic Radiology and Nuclear
           Medicine, 267.

(Ph75a)   Phelps, M.E., Gado, M.H. and Hoffman, E.J., 1975, Radiology, 117,
           585.

(Ph75b)   Phelps, M.E., Hoffman, E.J., and Ter-Pogossian, M.M., 1975,
           Radiology, 117, 573.

(Pi78)   "Picker Announces One Second CT Scanning," 1978, Picker, Inc.

(Pr64)   Price, W.J., 1964, Nuclear Radiation Detection.

(Pr78)   "Proposed Recommendations for Diagnostic Radiology Facilities
           Quality Assurance Programs," 1978, Federal Register, 43, 18157.

(Ra66)   Raju, M.R., 1966, Phys. Med. Biol., 11, 371.

(Re76)   "Regulations for the Administration and Enforcement of 'The
           Radiation Control for Health and Safety Act of 1978'," 1976,
           HEW/FDA 76-8035.

(Ro62)   Rosenweig, W., 1962, Rev. Sci. Instrum., 33, 379.

(Sc64)   Scharf, K. and Sparrow, J.H., 1964, J. Res. Nat. Bur. Stand.
           68A, 683.

(Sc66)   Scharf, K. and Sparrow, J.H., 1966, J. Res. Nat. Bur. Stand.,
           70A, 181.

(Sc67)   Scharf, K., 1967, Health Phys., 13, 575.

(Sc71)   Scharf, K. and Mohr, R.K., 1971, J. Res. Nat. Bur. Stand.,
           75A, 579.

(Sc78)   Schneider, R.H., 1978, in Proceedings of the 9th Annual National
           Conference in Radiation Control, 91.

(Se76)   "Searle Introduced Pho/Trax 4000 CT Scanner," 1976, Searle CT
           Systems, Inc.

(Sh78)   Shaw, J.E. and Thomas, R.L., 1978, Phys. Med. Biol., 23, 519.

(Sho78)   Showalter, C., 1978, personal communication.

(Si76)   Simon, S. and Hiller, G., 1976, "Silicon PIN Radiation Detectors,"
           Unitrode Corporation.

(So75)   "Solid State Silicon Photodiodes," 1975, Radio Corporation of
           America.

(Sp77)   "Specifications for 'Standard Model' Whole Body Scanners by
           Manufacturers," 1977, Radiol. Nucl. Med. Mag., 5, 22.

(Spi77)   Spital, R.D., 1977, in _Proceedings of the 1977 Digital Equipment Computer Users Society National Meeting_, 1399.

(St76)   Stout, D.F., 1976, _Handbook of Operational Amplifier Circuit Design_.

(St77)   "Standards and Criteria for Computerized Axial Tomography Scanner Certificate of Need and Section 1122 Approvals," 1977, Dept. of Health and Rehabilitative Services, Office of Community Medical Facilities, State of Florida.

(Su78)   Suzuki, A. and Suzuki, M., 1977, "Use of a Pencil-shaped Ionization Chamber for Measurement of Exposure Resulting from a Computed Tomography Scan," Capintec, Inc.

(Ta77)   Tavernas, J.M. and Wittenberg, J., 1977, in _Reconstruction Tomography in Diagnostic Radiology and Nuclear Medicine_, 425.

(Te73)   Teledyne--Philbrick, Inc., 1973, Bulletin AN-9.

(Th77)   "Therapy In-Vivo Dosimetry System for Irregular Field Dosimetry," 1977, Nuclear Associates, Inc.

(Th78)   Thomas, S.R., Schneider, A.J., Kereiakes, J.G., Lakin, R.R., Chambers, A.A. and Tomsick, T.A., 1978, _Med. Phys_, 5, 124.

(TL73)   "TLD-Personnel Dosimetry," 1973, in _Instrumentation for Environmental Monitoring--Radiation III_, 6.

(Tu77)   Turcke, D.A. and Gilmore, G.T., 1977, _Appl. Radiol._, 6, 149.

(Un78)   "Union Carbide Adds Body Version of Its Radionuclide Function Imager," 1978, _Radiol./Nucl. Med. Mag._, 8, 57.

(Va76)   "Varian Whole-Body CT Scanner," 1976, Varian Radiation Division.

(Va77)   "Varian Whole-Body-CT Scanner Specifications," 1977, Varian Radiation Division.

(Vi78)   "Victoreen Model 550-Radocon III," 1978, Victoreen Corp.

(We77)   Weinstein, M.A., Duchesneau, P.M. and McIntyre, W.J., 1977, _Radiology_, 122, 699.

(Wh63)   Whelpton, D. and Watson, B.W., 1963, _Phys. Med. Biol._, 8, 33.

(Ya78)   Yalcintas, G., 1978, paper given at 1978 National Health Physics Society Meeting.

(Za77)   Zatz, L.M., 1977, in _Reconstruction Tomography in Diagnostic Radiology and Nuclear Medicine_, 245.

(Zi62)   Ziemba, F.P., Pelt, G., Ryan, G., Wang, L., and Alexander, R., 1962, _I.R.E. Trans. Nucl. Sci._, NS-9, 155.

BIOGRAPHICAL SKETCH

John Joseph Lanza was born August 18, 1953, in San Antonio, Texas.
A few months after birth, he left the United States for Great Britain
and remained there for three years. In 1956, he returned to America
and lived in Delaware and New York. He again journeyed to Great Britain
in 1958 and, subsequently, returned home in 1961. After completing his
elementary and intermediate education in various locations throughout
the country, he attended high school in Cocoa, Florida, where he gradu-
ated magna cum laude in 1971.

He began his higher-education at Brevard Community College in
Cocoa, Florida, where he graduated in 1973 with an Associate of Arts
degree in pre-engineering studies. During these two years, he first
worked at the Cocoa/Rockledge Country Club as a chef and then, later,
at Wuesthoff Memorial Hospital, Rockledge, Florida, as a nursing
assistant and as a psychiatric technician.

In September, 1973, he matriculated at the University of Florida
in Gainesville, Florida, as a junior. In this first year, he was in-
volved in a research project investigating the fluid-flow properties
of blood in the cardiac arteries. During the summer of 1974, he worked
as a laboratory technician at Wuesthoff Memorial Hospital.

He returned to the University of Florida in September, 1974, and
obtained a part-time job as a laboratory technician at the Shands
Teaching Hospital. In June, 1975, he graduated from the University

of Florida with a Bachelor of Science degree in bio-medical electrical
engineering.

Immediately after completing his undergraduate education, he entered
graduate school in nuclear engineering sciences and received a Master of
Science degree with a concentration in health physics in June, 1976.
The title of his special project was "The Health Physics Aspects of the
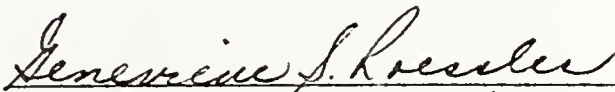Fusion-Fission Hybrid Reactor."

Following completion of his M.S. requirements, he initiated research
on a Ph.D project that was ultimately funded by the Bureau of Radiologi-
cal Health. After graduation, he intends to seek employment in the field
of medical radiation physics.

I certify that I have read this study and that in my opinion it conforms to acceptable standards of scholarly presentation and is fully adequate, in scope and quality, as a dissertation for the degree of Doctor of Philosophy.
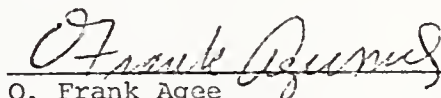
Walter Mauderli, Chairman
Professor of Nuclear Engineering
Sciences

I certify that I have read this study and that in my opinion it conforms to acceptable standards of scholarly presentation and is fully adequate, in scope and quality, as a dissertation for the degree of Doctor of Philosophy.
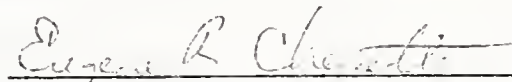
Genevieve S. Roessler, Co-Chairman
Assistant Professor of Nuclear
Engineering Sciences

I certify that I have read this study and that in my opinion it conforms to acceptable standards of scholarly presentation and is fully adequate, in scope and quality, as a dissertation for the degree of Doctor of Philosophy.

O. Frank Agee
Professor of Radiology

I certify that I have read this study and that in my opinion it conforms to acceptable standards of scholarly presentation and is fully adequate, in scope and quality, as a dissertation for the degree of Doctor of Philosophy.

Eugene R. Chenette
Professor of Electrical Engineering

I certify that I have read this study and that in my opinion it conforms to acceptable standards of scholarly presentation and is fully adequate, in scope and quality, as a dissertation for the degree of Doctor of Philosophy.

Lawrence T. Fitzgerald
Assistant Professor of Nuclear
Engineering Sciences

This dissertation was submitted to the Graduate Faculty of the College of Engineering and to the Graduate Council, and was accepted as partial fulfillment of the requirements for the degree of Doctor of Philosophy.

March 1979

Dean, College of Engineering

Dean, Graduate School